IEEE Access
Multidisciplinary ⋮ Rapid Review ⋮ Open Access Journal

Received 27 May 2024, accepted 11 June 2024, date of publication 19 June 2024, date of current version 27 June 2024.

Digital Object Identifier 10.1109/ACCESS.2024.3416809

RESEARCH ARTICLE

Novel Market-Based Mechanism for Flexibility Provision by Water Distribution Networks to Power Systems

A. BELMONDO BIANCHI[1], (Student Member, IEEE), M. A. PARDO[2], T. ALSKAIF[3], (Senior Member, IEEE), H. H. M. RIJNAARTS[1], AND S. SHARIAT TORBAGHAN[1], (Senior Member, IEEE)

[1]Department of Environmental Technology, Wageningen University and Research, 6708 PB Wageningen, The Netherlands
[2]Department of Civil Engineering, University of Alicante, 03690 Alicante, Spain
[3]Department of Information Technology, Wageningen University and Research, 6708 PB Wageningen, The Netherlands

Corresponding author: A. Belmondo Bianchi (alessio.belmondobianchidilavagna@wur.nl)

This work was supported in part by the Research Program AquaConnect, funded by the Dutch Research Council [Nederlandse Organisatie voor Wetenschappelijk Onderzoek (NWO)] under Grant-ID P19-45, in part by public and private partners of the AquaConnect Consortium and coordinated by Wageningen University and Research, in part by the Research Project "DESarrollo de herramientas de optimización para reducir los consumos ENergéticos y de emisiones en REdes de Distribución de Agua a presión (DESENREDA)" through the 2021 call "Estancias de Movilidad en el Extranjero Jose Castillejo" of the Ministerio de Universidades under Grant CAS21/00085, and in part by the project "Hi-Edu Carbon" Erasmus Plus Program, Key Action and Action Type under Grant KA22021 and Grant 2021-1-SK01-KA220-HED-000023274.

ABSTRACT Large-scale integration of renewable energy sources with their intermittent output is introducing new challenges for system operators. The challenge arises from imperfect wind and solar forecasts that lead to deviations in electricity production in real time. This has urged system operators to explore new sources of flexibility including the water sector. Along with these advancements, municipalities are becoming increasingly interested in coordinating water and energy systems in urban areas. This study introduces a novel market-based mechanism for harnessing flexibility from an integrated water and power system. The mechanism is formulated as a data-driven distribution robust chance-constrained program. It coordinates the operation of flexible power generators and water pumps through affine policies, regulating the participation of flexible assets in day-ahead and real-time market segments. Water flows are approximated through a novel convex hull-based relaxation technique. This results in a second-order cone program that allows the power system operator to leverage demand-side flexibility from the water network. The fluctuating water demands, derived from direct consumption measurements, are considered to ensure seamless integration with renewable energy sources. The water distribution network is explored for its potential to offer flexibility services, such as demand response to the power network. The mechanism is tested on a real case study in Alicante, Spain, to determine effective water-energy regulation policies and identify potential cost savings.

INDEX TERMS Demand-side flexibility, distribution robust chance constraints, market-based mechanism, water-energy coordination, wind-solar energy.

NOMENCLATURE

Abbreviations

ADMM	Alternating direction method of multipliers.
CC	Chance-constraint.
DA	Day-ahead.
DC − OPF	Direct current optimal power flow.
DR	Demand-response.
DRCC	Distribution robust chance-constraint.
KW	Kilowatt.
KWh	Kilowatt-hour.
MAE	Mean absolute error.
MCP	Market-clearing price.
MISOCP	Mixed-integer second-order cone program.

The associate editor coordinating the review of this manuscript and approving it for publication was Wencong Su.

PN	Power network.
PV	Photovoltaic.
PVC	Polyvinyl chloride.
QCQP	Quadratically-constrained quadratic program.
RES	Renewable energy sources.
RT	Real-time.
SBSP	Scenario-based stochastic programming.
SO	System operator.
SOC	Second-order cone.
SOCP	Second-order cone program.
WN	Water network.

Number sets

$\mathbb{R}$	Real numbers.
$\mathcal{D}$	Conventional power loads.
$\mathcal{E}$	Pressurized water pipes.
$\mathcal{G}$	Conventional generators.
$\mathcal{J}$	Water network junctions.
$\mathcal{L}$	Power lines.
$\mathcal{N}$	Power buses.
$\mathcal{P}$	Centrifugal variable speed pumps.
$\mathcal{R}$	Water reservoirs.
$\mathcal{S}$	Elevated water storage tanks.
$\mathcal{T}$	Number of time slots.
$\mathcal{W}$	Renewable power generators.
$\mathcal{Z}$	Number of random variables.
Π	Ambiguity set.

Symbols

$\aleph_{i,j,t}$	Relative rotational speed of pump (i,j) at time t.
$\alpha_{e,t}$, $\beta_{u,t}$	Flexibility offered by generator e and pump u at time t.
$\breve{}$	Symbol denoting uncertainty-dependent counterparts of the decision variables.
$\Delta h^{ref,DA}$, Δh^{DA}	Reference and actual pressure head gain of pump (i,j) at time t in DA (Algorithm 1).
$\Delta h^{ref,RT}$, Δh^{RT}	Reference and actual pressure head gain of pump (i,j) at time t in RT (Algorithm 1).
Δ_t	Vector of random forecast errors at time t.
$\delta_{i,j,t}$	Adjustment factor for change in power consumption of pump (i,j) at time t.
ϵ	Violation probability level for individual DRCCs.
$\epsilon^{'}$	Measure of confidence in the SOC reformulation of DRCCs.
γ_t	Aggregated forecast error of renewable generators at time t.
$\mathbb{E}_{\mathbb{P}}$	Expectation operator under probability distribution $\mathbb{P}$.
$\mathbb{P}$	Worst-case distribution of uncertainty selected from the ambiguity set Π.
μ^{Π}	Mean vector of forecast errors.
$\omega_{i,t}$	Forecast error of renewable generator i at time t.
ϕ^T	Transpose vector of ones.
Σ	Covariance matrix of forecast errors.
Σ_t	the t-th diagonal sub-matrix of the covariance matrix Σ at time t.
τ	Length of time step t.
$\theta_{n,t}$	Voltage angle of bus n at time t.
$\underline{\aleph}_{i,j}$, $\overline{\aleph}_{i,j}$	Relative minimum and maximum rotational speeds of pump (i,j).
$\underline{f}_{n,m}$, $\overline{f}_{n,m}$	Lower and upper power flow limits through line (n,m).
$\underline{H}_s^{end}$, $\overline{H}_s^{end}$	User-selected minimum and maximum level of storage tank s at the end of the simulation ($t = end$).
$\underline{P}_{l,t}^D$, $\overline{P}_{l,t}^D$	Lower and upper bounds for conventional load l at time t.
$\underline{P}_e^G$, $\overline{P}_e^G$	Lower and upper bounds for conventional power generator e.
$\underline{P}_{w,t}^W$, $\overline{P}_{w,t}^W$	Lower and upper bounds for renewable generator w at time t.
$\underline{Q}_{i,j}$, $\overline{Q}_{i,j}$	Minimum and maximum flow through pipe/pump (i,j) at time t.
Υ	Threshold percentage for termination condition of Algorithm 1.
$\zeta_{i,j,t}^s$, $\zeta_{i,j,t}^p$	Auxiliary variables for SOC relaxation of friction head losses and pump energy consumption.
A_s	Cross-sectional area of storage tank s.
$a_{i,j}$, $b_{i,j}$, $c_{i,j}$	Hydraulic parameters of pump (i,j).
$B_{n,m}$	Susceptance of power line (n,m).
C_e^G	Marginal production cost of generator e.
C_e^{Av}, C_u^{Av}	Availability cost of generator e and pump u.
E_0	Base voltage of the power system.
$F_{i,j}$	Fixed part of Darcy-Weisbach equation for pipe (i,j).
g, ρ, $\eta_{i,j}$	Gravitational acceleration, density of water, and efficiency of pump (i,j).
$h_{j,t}$, $h_{r,t}$, $h_{s,t}$	Pressure head in junction j, reservoir r and storage tank s at time t.
$m_{i,j,t}$	Auxiliary variable for the McCormick relaxation of bilinear term (i,j) at time t.
$p_{l,t}^D$	Power demand of conventional load l at time t.
$p_{e,t}^G$	Power produced by generator e at time t.
$p_{u,t}^P$	Power demand of pump load u at time t.
$P_{i,j,t}$	Energy consumption of pump (i,j) at time t.
$q_{i,j,t}^L$, $q_{i,j,t}^U$	Lower and upper water flow bounds for the McCormick envelope.
$r_{i,j}^0$, $r_{i,j}^1$	Parameters defining the convex envelope of the friction head losses for pipe (i,j).
U_l^D	Bid of conventional load l.
U_u^P	Bid of pump load u.
$x_{i,j}$, $y_{i,j}$, $z_{i,j}$	Empirical parameters describing the energy consumption of pump (i,j).

$d_{j,t}$	Water demand in junction j at time t.
$f_{n,m,t}$	Power flow from bus n to bus m at time t.
$H_j^0, \underline{H}_j, \overline{H}_j$	Elevation, minimum and maximum pressure head in junction j.
$H_s^0, h_s^0, \underline{H}_s, \overline{H}_s$	Elevation and initial, minimum and maximum level in storage tank s.
$p_{w,t}^W$	Power produced by renewable generator w at time t.
$q_{i,j,t}$	Water flow from node i to node j at time t.

I. INTRODUCTION

Global energy demand is increasing, with projections up to 2040 indicating an annual economic growth rate of 3.4% and an anticipated rise of approximately 30% [1]. Alongside this demand surge, the integration of Renewable Energy Sources (RES), such as wind and solar, in power networks is posing challenges due to their variability and location-dependence, complicating power flow control and network stability [2], [3]. To address these challenges, System Operators (SO) must develop cost-efficient approaches to manage the uncertainties associated with the rise in RES, including exploring new sources of flexibility. One potential source of flexibility is the water sector.

The water sector constitutes a vital infrastructure that accounts for approximately 4% of global electricity consumption [1], [4]. Water and wastewater treatment plants, which use 25-30% of total water-related energy consumption [5], incur significant electricity costs, particularly in pumping drinking water, which can represent up to 50% of operational costs [6]. Given the environmental concerns, escalating energy costs, and advancements in renewable energy technologies, the integration of RES in power systems is gaining momentum [7]. This shift is also being considered by operators of water and electricity networks, although it introduces uncertainty. Flexibility becomes crucial in this context, referring to the ability of systems to adapt to changing conditions and ensure reliable and efficient power and water supply [8]. In the water sector, flexibility entails sustaining operations during challenging scenarios by storing water in intermediate reservoirs to ensure continuous water supply despite fluctuations in energy or water sources. In the power sector, flexibility involves adjusting load and generation through methods such as flexible generation, Demand-response (DR), energy storage, and sector integration [9], [10].

The competitive advantage of the Water Network (WN) lies in its abundant flexibility capacity, which results from over-sized asset capacities and large inertia resulting from water reserves. Therefore, although the water network has rather a small energy footprint, it has abundant flexibility at its disposal which makes it an important candidate for providing flexibility services to the power systems as a DR provider [11]. From the water system viewpoint, addressing the energy intensity of water distribution networks is crucial for reducing their cost and environmental impact. In this context, enhancing sector integration presents the dual potential of furnishing flexibility to the Power Network (PN) and fostering enhanced energy efficiency and resilience within the WN. The coordination between water and power networks is crucial for a dependable and sustainable supply of resources under changing conditions and challenges.

Researchers have worked to improve pressurized water networks in cities by reducing water usage [12], managing infrastructure [13], lowering pressure [14], and cutting energy costs. Literature has investigated the energy footprint in the urban water cycle, ranging from 0.21 to 4.07 kWh/m^3 [15]. The amount varies based on factors such as location, water source, climate, and treatment methods. Similar efforts have been undertaken in power networks to optimize electricity transmission and distribution systems and enhance overall efficiency. These include, implementing smart grids and demand response mechanisms [16], integrating RES [17], reducing energy losses [18], improving grid stability and resilience [19], forecasting and managing electricity loads [20], and ensuring power quality and voltage regulation [21]. The above studies aim to address resource use efficiency, mitigate operational costs, and promote sustainability within their respective infrastructures. However, research concerning the development of coordination mechanisms for integrated power and water networks remains limited. Such an integrated approach holds great significance for achieving even greater economic efficiency and optimizing resource utilization across interconnected urban systems.

Models and technologies have been proposed to explore synergies between the water and energy sectors. Hydraulic tanks have been identified as efficient devices for water and energy storage [22], while pumps and turbines offer further opportunities for synergy [23], [24]. Moreover, consistent water flow and minimal pump operation can reduce energy consumption in pressurized water networks [25]. However, modelling integrated power and water networks presents considerable challenges because of the non-convex nature of both power and water physics. Focusing on the WN only, the model developed by [26] is a Mixed-integer Second-order Cone Program (MISOCP) designed for energy-optimal pump scheduling and water flow, demonstrating the capacity to enhance energy efficiency within the water sector. A follow-up work in [27] demonstrated the potential for using water supply networks for harvesting renewable energy. However, these models assumed fixed electricity prices and overlooked the dynamics of the PN, thus failing to account for the impacts that the water network's operation may have on the PN and vice versa.

Integrated energy and water modelling can be challenging due to the non-linear and non-convex nature of both power and water flows as well as the non-linear operating profile of water pumps. In this regard, [28] formulates an integrated power and water coordination mechanism as a non-convex Quadratically-constrained Quadratic Program (QCQP). The

model optimizes controllable assets across both networks. They propose a distributed optimal solution approach for the optimal water-power flow problem based on the alternating direction method of multipliers (ADMM). In [29], the authors introduced a quasi-convex hull relaxation technique for the optimal water-power flow problem and developed a coordination mechanism for demand-side management in the PN. They demonstrated that grid flexibility could benefit from controllable water pump loads. However, these models did not consider the inherent uncertainties in power and water networks, such as uncertainties associated with power and water demands, as well as RES generation.

The work in [30] proposed a chance-constrained power and water coordination mechanism that incorporates pumps as flexible loads in the PN. Their study accounts for demand uncertainties (such as power loads and water demands) but not supply uncertainties (such as RES generation). The probabilistic chance constraints (CC) are approximated using the scenario-based stochastic programming (SBSP) approach. This approach requires a large number of scenarios to achieve a good representation of the uncertainty, which can be computationally intensive to simulate. In a follow-up work [31], the authors derived the analytical reformulation of the CC for the integrated power-water flow problem. While this approach is computationally tractable, it requires assumptions on the underlying probability distribution which is often unknown.

The work presented in [32] introduces an adaptive robust water pumping problem aimed at managing power demand uncertainty while providing voltage support and frequency regulation. Their findings suggest that the adaptive robust approach, when compared to the conventional robust approach, is less conservative. However, a notable drawback is its reliance on known uncertainty distributions, which may not be known in practice. Additionally, the sequential formulation utilized to solve the adaptive robust optimization problem fails to capture the trade-offs between the cost of pump scheduling in the Day-ahead (DA) market and the profits from frequency regulation services in the Real-time (RT) market. Another limitation of the works presented in [30], [31], and [32] is the use of a linear function to model pump power consumption, which is suitable for fixed-speed pumps. However, fixed-speed pumps are constrained to a limited range of operating points, thereby limiting their flexibility when compared to variable-speed pumps. In cases where variable-speed pumps are employed, such as in [33], they are modelled using piecewise linear approximations. Researchers acknowledge that this approach tends to introduce computational complexity, especially in large-scale systems.

The aforementioned studies aim to optimize controllable assets in both power and water networks but often fall short of capturing their dynamics and uncertainties. These studies frequently overlook electricity market dynamics, assuming fixed prices and neglecting crucial aspects such as DA and RT market segments. Therefore, a comprehensive formulation and modelling approach is necessary to study decision-making in integrated power and water networks, incorporating their dynamics in both DA and RT markets. These two segments of the power market offer the adequate price signals that are crucial for a DR program, such as the WN, to perform a successful market-based energy arbitrage. The intended problem formulation should account for the physical characteristics of both networks and the financial considerations associated with operating the two sectors. As such, it should provide decision solutions with techno-economic interpretations, resolving operational challenges arising from short-term uncertainties.

This study proposes a novel market-based coordination mechanism for integrated power and water networks, considering short-term scheduling and operation. We assume that flexibility is sourced by flexible generators and variable-speed pumps (operating as flexible loads). The proposed model seeks to maximize utility in the power sector while maintaining flexibility to address potential power imbalances in RT. At the same time, it seeks to ensure the reliable operation of the WN. We consider wind and solar power forecasts as the sources of uncertainty. The problem is formulated as a Data-driven Distribution Robust Chance-constrained program (DRCC). Convex approximations and affine control policies are employed for computational traceability, resulting in a Second-order Cone Program (SOCP). The innovation lies in formulating a DRCC program for integrated power and water networks with uncertainty in RES generation. As a sequel to our previous work [34], an improved relaxation technique is proposed for friction head losses and pump energy consumption functions. In addition, we develop a novel iterative solution algorithm to capture the dynamics of variable speed pumps. The model identifies synergies between interdependent power and water networks and suggests a market participation mechanism for flexible water pumps in the power system. This study provides valuable insights for utility operators and practitioners during the planning and operation phases of power and water networks. The contributions of the paper can be summarized as follows:

1) Proposes a novel market-based coordination mechanism for procuring flexibility from the water network. This mechanism allows for effectively procuring flexibility from the water system to contain imbalances caused by imperfect wind and solar forecasts in the power network.
2) Formulates the problem as a novel augmented distribution-robust chance-constrained market clearing problem, operating within a centralized and fully competitive market set-up.
3) Introduces a novel convex relaxation technique and iterative solution algorithm to convexity water network hydraulic constraints to enhance problem tractability.

The rest of the paper is organized as follows. Section II presents the problem formulation. Section III discusses the solution methodology. Section IV introduces the case study.

Section V discusses the numerical results. Section VI presents the conclusions and the future work.

II. MATERIAL AND METHODS

A. MODELLING ASSUMPTIONS

The WN is described as a directed graph comprising nodes $\mathcal{I}$ and edges $\mathcal{E}$, with nodes categorized as junctions ($j \in \mathcal{J}$), reservoirs ($r \in \mathcal{R}$), or elevated storage tanks ($s \in \mathcal{S}$), such that $\mathcal{I} = \mathcal{J} \cup \mathcal{R} \cup \mathcal{S}$. Reservoirs are considered infinite water sources, while tanks have finite volumes. Compensation or head tanks, serving as storage units for both water and energy, offer a means of water storage. As a result, water can be pumped into these tanks during specific intervals and subsequently discharged, harnessing gravitational potential energy, at later times. The WN edges represent water pipes and variable speed pumps $(i, j) \in \mathcal{P}$ with $\mathcal{P} \subset \mathcal{E}$.

On the power side, a PN is considered, comprising power lines $\mathcal{L}$ and nodes $\mathcal{N}$ with uncontrollable loads $l \in \mathcal{D}$, controllable pump loads $u \in \mathcal{P}$, conventional power generating units $e \in \mathcal{G}$, and RES $w \in \mathcal{W}$. The study assumes that water pumps, along with storage tanks, act as flexible loads in the PN. Moreover, power generators can function as flexible assets by adjusting power production within operational limits. In this context, flexibility is defined as the capability of adjusting generation or consumption levels in response to changes in RES availability. Given our focus on flexible power generators, such as gas-fired power plants, we do not consider the ramp-up and down limits of these generators in our analysis. These flexible units can adjust their operations, allowing them to provide the necessary support to the grid without being constrained by ramp rates.

The PN modelling approach adopts a linearized DC Optimal Power Flow (DC-OPF) formulation, assuming voltage magnitudes close to 1 per unit, neglecting power losses, and considering small resistance compared to reactance. It must be noted that the linearized DC-OPF formulation of the power system is sub-optimal. However, we believe that our approach has significant merits for the following reasons. Firstly, the reactive power consumption of electric motors is not priced in the current electricity market structure [35]. Therefore, our focus is on active power, aligning with the objectives of this study and current economic considerations. Secondly, including nonlinear reactive power constraints would make the problem significantly more challenging, both mathematically and computationally [36]. Since we aim to investigate the potential of an integrated water and power network in managing uncertainty in renewable power generation within an electricity market setup, we believe our power network modelling approach is sufficiently accurate for the current study.

The model focuses on wind and solar power production as the sources of uncertainty. Wind and solar forecast scenarios are obtained from the forecasting tool RESGen [37] as depicted in Figure 1. Based on several generated scenarios,

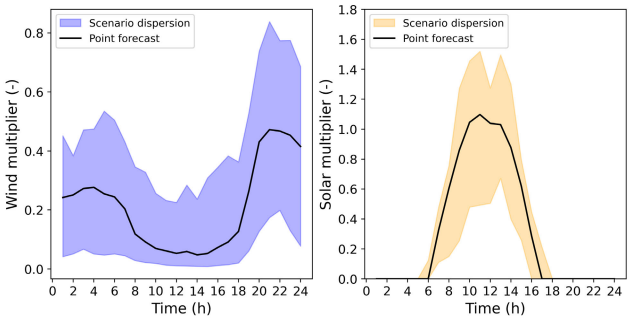

FIGURE 1. Wind and solar data obtained from RESGen. The shaded area captures varying wind and solar power forecast scenarios. The point forecast is depicted by the black line.

uncertainty is represented using a moment-based ambiguity set. This set characterizes the uncertainty arising from forecast errors in DA wind and solar power predictions. Following previous studies [38], [39], the forecast errors are assumed to follow an unknown multivariate probability distribution. To encompass the overall system uncertainty, a vector of random variables $\Delta = [\omega_{1,1}, \omega_{2,1}, \ldots, \omega_{i,t}] \in \mathbb{R}^Z$ is defined, where i and t represent specific space and time dimensions. The moment-based ambiguity set Π contains all probability distributions described by known parameters, namely the mean (μ^Π) and covariance (Σ^Π) of the forecast errors:

$$\Pi = \mathbb{P} \in \Pi_0(\mathbb{R}^Z) : \mathbb{E}_\mathbb{P}[\Delta] = \mu^\Pi,\ \mathbb{E}_\mathbb{P}[\Delta\Delta^T] = \Sigma^\Pi.$$

The expectation with respect to the probability distribution is denoted by $\mathbb{E}_\mathbb{P}$, and the transpose operator is represented by ^{T}. It is assumed that the mean is zero and the covariance matrix can be estimated from empirical data of wind and solar forecast errors. The total deviation from the DA forecast of wind turbines and Photovoltaic (PV) panels at a given time is determined by the dot product of the unit vector ϕ^T and the forecast error vector Δ_t, where a non-negative value indicates a shortage of RES during RT operation compared to the DA point forecast.

In this study, we have opted for the DRCC approach because of its specific advantages over SBSO. Firstly, the DRCC approach does not require assumptions about the underlying probability distribution, making it suitable for cases where errors from imperfect forecasting algorithms may lack a specific probability distribution. Secondly, the DRCC approach is computationally more efficient than scenario-based stochastic programming. The main differences between SBSO and DRCC lie in uncertainty modelling, solution approach, and computational burden. SBSO relies on identifying the underlying probability distribution of random variables, such as wind and solar forecasts, and involves solving numerous scenarios projected from the identified probability distribution using techniques like Monte Carlo simulation or scenario trees. This process can become computationally expensive as uncertain factors increase or

scenarios become more complex, especially when variables are interdependent or in dynamic optimization cases.

In contrast, DRCC defines an uncertainty set encompassing possible random variable realizations and optimizes an objective considering the worst-case realization within this set, leading to a solution that satisfies constraints with a certain probability. The computational complexity of DRCC depends on the chosen uncertainty set and the specific optimization algorithm. Although DRCC may yield more conservative solutions, it outperforms SBSO in computational efficiency for large problems with many random variables, complex scenarios, poorly defined uncertainty, or when risk assessment is not intended. For detailed comparisons of SBSO and DRCC for different problems and system sizes, we refer to [40], [41], and [42].

B. MATHEMATICAL FORMULATION OF THE PROBLEM

The proposed DRCC program is formulated as follows (1)-(21). The objective function (1) follows a min-max structure, minimizing the total social cost of the power system while drawing uncertainty from the worst-case probability distribution. As such, the problem also maximizes the expected social cost that could occur due to worst-case uncertainty realization.

$$\underset{\Gamma,\mathbb{P}\in\Pi}{MinMax}\ \mathbb{E}_{\mathbb{P}}\left[\sum_{t\in\mathcal{T}}\left(\sum_{e\in\mathcal{G}}C_e^G(p_{e,t}^G)-\sum_{l\in\mathcal{D}}U_l^D p_{l,t}^D-\sum_{u\in\mathcal{P}}U_u^P p_{u,t}^P\right)\right] \quad (1)$$

$$s.t.\ h_{r,t}=H_{r,t}^0\ r\in\mathcal{R},t\in\mathcal{T} \quad (2)$$

$$\sum_{i\in N_{in}J}q_{i,j,t}-\sum_{k\in N_{out}J}q_{j,k,t}=d_{j,t}\ j\in\mathcal{J},t\in\mathcal{T} \quad (3)$$

$$h_{s,t}-h_s^0=\frac{\tau}{A_s}\left(\sum_{i\in N_{in}s}q_{i,s,t}-\sum_{j\in N_{out}s}q_{s,j,t}\right)\ s\in\mathcal{S},t=1 \quad (4)$$

$$h_{s,t}-h_{s,t-1}=\frac{\tau}{A_s}\left(\sum_{i\in N_{in}s}q_{i,s,t}-\sum_{j\in N_{out}s}q_{s,j,t}\right)$$
$$s\in\mathcal{S},t>1 \quad (5)$$

$$h_{i,t}-h_{j,t}=F_{i,j}(q_{i,j,t})^2\ (i,j)\in\mathcal{E},t\in\mathcal{T} \quad (6)$$

$$h_{j,t}-h_{i,t}=a_{i,j}q_{i,j,t}^2+b_{i,j}q_{i,j,t}+c_{i,j}\ (i,j)\in\mathcal{P},t\in\mathcal{T} \quad (7)$$

$$P_{i,j,t}=\frac{g\rho\tau}{\eta_{i,j}}(h_{j,t}-h_{i,t})q_{i,j,t}\ (i,j)\in\mathcal{P},t\in\mathcal{T} \quad (8)$$

$$\underset{\mathbb{P}\in\Pi}{min}\mathbb{P}[\underline{H}_j+H_j^0\le h_{j,t}\le\overline{H}_j+H_j^0]\ge(1-\epsilon)$$
$$j\in\mathcal{J},t\in\mathcal{T} \quad (9)$$

$$\underset{\mathbb{P}\in\Pi}{min}\mathbb{P}[\underline{H}_s+H_s^0\le h_{s,t}\le\overline{H}_s+H_s^0]\ge(1-\epsilon)$$
$$s\in\mathcal{S},t\in\mathcal{T} \quad (10)$$

$$\underset{\mathbb{P}\in\Pi}{min}\mathbb{P}[\underline{H}_s^{end}\le h_{s,t}\le\overline{H}_s^{end}]\ge(1-\epsilon)\ s\in\mathcal{S},t=end \quad (11)$$

$$\underset{\mathbb{P}\in\Pi}{min}\mathbb{P}[\underline{Q}_{i,j}\le q_{i,j,t}\le\overline{Q}_{i,j}]\ge(1-\epsilon)\ (i,j)\in\mathcal{E},t\in\mathcal{T} \quad (12)$$

$$\underset{\mathbb{P}\in\Pi}{min}\mathbb{P}[\underline{Q}_{i,j}\le q_{i,j,t}\le\overline{Q}_{i,j}]\ge(1-\epsilon)\ (i,j)\in\mathcal{P},t\in\mathcal{T} \quad (13)$$

$$\underline{P}_{l,t}^D\le p_{l,t}^D\le\overline{P}_{l,t}^D\ l\in\mathcal{D},t\in\mathcal{T} \quad (14)$$

$$\underline{P}_{w,t}^W\le p_{w,t}^W\le\overline{P}_{w,t}^W\ w\in\mathcal{W},t\in\mathcal{T} \quad (15)$$

$$\sum_{e\in\psi_{G_n}}p_{e,t}^G+\sum_{w\in\psi_{W_n}}p_{w,t}^W=\sum_{l\in\psi_{D_n}}p_{l,t}^D$$
$$+\sum_{u\in\psi_{P_n}}p_{u,t}^P+\sum_{m\in\Omega n}f_{n,m,t}\ n\in\mathcal{N},t\in\mathcal{T} \quad (16)$$

$$f_{n,m,t}=E_0^2B_{n,m}(\theta_{n,t}-\theta_{m,t})\ (n,m)\in\mathcal{L},t\in\mathcal{T} \quad (17)$$

$$\theta_{n,t}=0\ n=ref,t\in\mathcal{T} \quad (18)$$

$$p_{u,t}^P=P_{i,j,t}\ u\in\psi_{i,j}^P,(i,j)\in\mathcal{P},t\in\mathcal{T} \quad (19)$$

$$\underset{\mathbb{P}\in\Pi}{min}\mathbb{P}[\underline{P}_e^G\le p_{e,t}^G\le\overline{P}_e^G]\ge(1-\epsilon)\ e\in\mathcal{G},t\in\mathcal{T} \quad (20)$$

$$\underset{\mathbb{P}\in\Pi}{min}\mathbb{P}[\underline{f}_{n,m}\le f_{n,m,t}\le\overline{f}_{n,m}]\ge(1-\epsilon)\ (n,m)\in\mathcal{L},t\in\mathcal{T} \quad (21)$$

$\Gamma=h_{i,t},h_{r,t},q_{i,j,t},h_{s,t},P_{i,j,t},p_{l,t}^D,p_{w,t}^W,p_{e,t}^G,p_{u,t}^P,f_{n,m,t},\theta_{n,t}$ is the set of optimisation decision variables. Objective (1) minimizes the total expected social cost of the power system. Parameters U_l^D, U_u^P, and C_e^G represent the estimated bids of conventional load l, pump load u, and the marginal production cost of generator e, respectively. The objective function excludes power generation from wind and solar power producers as it assumes zero marginal production cost for RES. Additionally, water pump bids U_u^P are set at the maximum auction price (i.e., price cap or the bid with the highest price) to ensure full dispatch of pump loads for water supply-demand matching at all times.

Constraints (2)-(13) delineate the WN. Constraint (2) enforces a fixed head at the reservoir, where variable $h_{r,t}$ denotes the pressure head at reservoir r at time t. The flow balance in the network is maintained through constraint (3), which ensures that at any junction j and time t, the total inflow minus the total outflow equals the water demand, denoted by the variable $d_{j,t}$. The variable $q_{i,j,t}$ represents the water flow from node i to node j at time t. The tank level equations are described by constraints (4) and (5), governing the change in the level of storage tank s over time t represented by the variable $h_{s,t}$. The parameters τ and A_s are the time step and cross-sectional area of the tank, respectively. Constraint (6) accounts for the pipe friction head loss in the network. The variables $h_{i,t}$ and $h_{j,t}$ represent the pressure head at nodes i and node j at time t, respectively. Parameter $F_{i,j}$ is the fixed, flow-independent part of the Darcy-Weisbach equation. Pump hydraulic head gain is captured by constraint (7), where parameters $a_{i,j}$, $b_{i,j}$, and $c_{i,j}$ describe the hydraulic behaviour of pump (i,j). Constraint (8) defines the pump energy consumption ($P_{i,j,t}$) as a function of pump head gain and flow rate. Parameters ρ, g, and

$\eta_{i,j}$, denote the density of water, gravitational acceleration, and efficiency of pump (i,j), respectively. Constraints (9), (10), and (11) define the pressure head limits and minimum and maximum tank levels. Parameters H_j^0, $\underline{H}_j$, $\overline{H}_j$, $\underline{H}_s$ and $\overline{H}_s$ provide elevation, head, and tank level upper and lower limits. Parameters $\underline{H}_s^{end}$ and $\overline{H}_s^{end}$ provide the desired minimum and maximum tank level at the end of the time horizon. Constraints (12) and (13) define the pipe and pump flow limits. Parameters $\underline{Q}_{i,j}$ and $\overline{Q}_{i,j}$ represent the minimum and maximum flow through a pipe or pump (i,j).

Constraints (14) to (21) delineate the PN. Constraints (14) and (15) establish the limits for load and RES generation. They ensure that the power produced by wind or solar farms ($p_{w,t}^W$), and the electricity demand from loads ($p_{l,t}^D$) are within the specified bounds at each time period t. The parameters $\overline{P}_{l,t}^D$ and $\underline{P}_{l,t}^D$ represent the upper and lower limits for electricity demand, respectively, while $\overline{P}_{w,t}^W$ and $\underline{P}_{w,t}^W$ represent the limits for wind or solar power generation. Constraint (16) represents the power balance in the network. It ensures that the total power generated by generators and RES, along with the electricity demand from loads and power consumed by water pumps ($p_{u,t}^P$), is balanced with the power flow in the transmission lines $f_{n,m,t}$ at each time period t. Constraint (17) defines the power flow from bus n to bus m at time t. The variable $f_{n,m,t}$ represents the power flow between nodes n and m. Parameter $B_{n,m}$ represents the susceptance of the transmission line connecting these nodes and E_0 represents the base voltage magnitude, assumed to be close to one per unit. Constraint (18) enforces a fixed voltage angle at the slack node. The variable $\theta_{n,t}$ represents the voltage angle at bus n at time t. Constraint (19) couples the pump power consumption $P_{i,j,t}$ from constraint (8) with the pump load on the PN $p_{u,t}^P$. Constraint (20) defines the limits for conventional generation. It ensures that the power output from conventional generators ($p_{e,t}^G$) remains within the specified upper and lower bounds given by parameters $\overline{P}_{e,t}^G$ and $\underline{P}_{e,t}^G$. Constraint (21) defines the power flow limit through the transmission lines. It ensures that the power flow between nodes n and m remains within the specified upper and lower bounds $\overline{f}_{n,m}$ and $\underline{f}_{n,m}$. Note that inequalities (9)-(13), (20), and (21) are modelled as DRCCs. This implies that at the optimal solution, the probability of meeting each constraint is modelled to have a confidence level of at least (1)-ϵ).

The DRCC program (1)-(21) is currently computationally intractable. Firstly, it contains an unknown and potentially infinite number of variables and constraints due to its probabilistic nature. Secondly, it involves nonlinear and non-convex constraints (6), (7), and (8). Regarding infinite dimensionality, by utilizing affine control policies, convex approximations, and duality theory, DRCC problems can be analytically reformulated as deterministic convex problems across various ambiguity sets [43]. Regarding nonlinear water network constraints, several studies have employed linearization and convex relaxation techniques. Convex models can provide a simplified yet accurate representation of the behaviour of complex systems under certain conditions, which is why they are widely used in engineering and systems analysis [44]. Their key advantages include simplicity, stability analysis, and fast simulation. References [29], [33], and [45] employed linearization terms for common water pressurized system parameters, including head losses in pipelines, pressure head increases of pumps, and pump power consumption functions. These studies confirmed the accuracy and computational efficiency of the convex relaxation and linearization methods. In this study, we develop a novel solution algorithm leveraging linearizations and convex relaxations specifically tailored to model the water network within the DRCC framework. We believe this novel method accurately captures the dynamics of the water system.

The analytical reformulation of DRCCs is discussed in Section II-C. The linearization and convex relaxation of non-convex constraints are presented in Section II-D. The final problem formulation and solution procedure are discussed in Section III.

C. ANALYTICAL REFORMULATION OF PROBABILISTIC DRCCS

In the first step towards computational tractability, we adopt recourse actions to represent the behaviour of flexible assets, characterizing their response in RT as affine functions of uncertainty. Specifically, as linear functions of aggregated wind and solar forecast errors. The RT response is calculated in the expectation for the worst-case distribution of RES forecast errors $\mathbb{E}_{\mathbb{P}}$ in the ambiguity set Π. The recourse actions are modelled via linear decision rules using the random vector $\Delta \in \mathbb{R}^Z$. The market operator is requesting these recourse actions to regulate the flexibility response in the coupled power and water network. This includes flexible generators, water pumps and associated power and water flows. We focus on the stochastic water flow variable as an example to demonstrate the concept of affine response to uncertainty. Water flow through pipes can be adjusted in response to uncertainty realization in RT. We model this behaviour as follows:

$$\tilde{q}_{i,j,t} = q_{i,j,t} + (\phi^T \Delta_t)\breve{q}_{i,j,t} \quad (i,j) \in (\mathcal{E} \cup \mathcal{P}), t \in \mathcal{T}. \tag{22}$$

In (22), $\tilde{q}_{i,j,t}$ represents the total stochastic water flow through pipe or pump (i,j) at time t. It comprises two components: the nominal water flow $q_{i,j,t}$ and the uncertainty-dependent water flow $\breve{q}_{i,j,t}$. The latter denotes the participation factor of water flow (i,j) in compensating for the total wind and solar power mismatch $\phi^T \Delta_t$ at time t.

Assuming an affine response to uncertainty and zero mean forecast error, we analytically reformulate the DRCCs as Second-Order Cone (SOC) constraints following the approach described in [46]. Let us define $(\phi^T \Delta_t)\breve{q} := \sqrt{\frac{1-\epsilon}{\epsilon}} ||\breve{q} \sum^{1/2}||_2$, which for the sake of brevity we write as $\epsilon' \gamma_t \breve{q}$ where $\epsilon' := \sqrt{\frac{1-\epsilon}{\epsilon}}$ and $\breve{q}\gamma_t := ||\breve{q} \sum^{1/2}||_2$. Then constraint (12) can be reformulated with the following SOC constraints:

$$\underline{Q}_{i,j} - q_{i,j,t} \leq \epsilon' \breve{q} \gamma_t \quad (i,j) \in (\mathcal{E} \cup \mathcal{P}), t \in \mathcal{T} \tag{23}$$

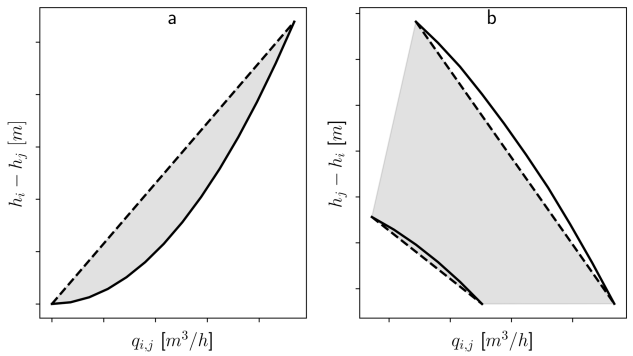

FIGURE 2. Convex approximations of the hydraulic system. (a) Darcy-Weisbach equation: solid line for true curve, dashed line for the linear segment, shaded area for the feasible domain. (b) Variable speed pump: solid lines for the actual curve, dashed lines for linear approximation, and shaded region for the feasible domain.

$$\overline{Q}_{i,j} - q_{i,j,t} \geq \epsilon' \breve{q} \gamma_t \quad (i,j) \in (\mathcal{E} \cup \mathcal{P}), t \in \mathcal{T}. \tag{24}$$

A similar procedure is adopted to reformulate the other probabilistic DRCCs of the program (1)-(21). The analytical reformulation of DRCCs enables a representation of the infinite-dimensional probabilistic problem into an equivalent deterministic problem. However, this approach does not suffice to make the problem computationally tractable. The problem still contains nonlinear and non-convex constraints (6), (7), and (8). A novel procedure to convexify these constraints is explained in Section II-D.

D. CONVEX RELAXATION OF HYDRAULIC CONSTRAINTS

Friction head losses in water pipes are commonly described using the non-convex Darcy-Weisbach equation (6). This is an equality constraint which models head losses as a quadratic function of the flow rate. To address this non-convexity, we follow the approach presented by [29] where constraint (6) is reformulated as the intersection of a convex function and a linear function such that $F_{i,j}\tilde{q}^2_{i,j,t} \leq \tilde{h}_{i,t} - \tilde{h}_{j,t} \leq r^0_{i,j} + r^1_{i,j}\tilde{q}_{i,j,t}$. This reformulation enables us to model the feasible region, enclosed between the resulting convex set, as shown in Figure 2a. Under the assumption of affine response to uncertainty, we describe this convex set by defining uncertainty-dependent and independent counterparts as follows:

$$h_{i,t} - h_{j,t} \geq F_{i,j} q^2_{i,j,t} \quad (i,j) \in \mathcal{E}, t \in \mathcal{T} \tag{25}$$

$$h_{i,t} - h_{j,t} \leq r^0_{i,j} + r^1_{i,j} q_{i,j,t} \quad (i,j) \in \mathcal{E}, t \in \mathcal{T} \tag{26}$$

$$\phi^T \Delta_t (\breve{h}_{i,t} - \breve{h}_{j,t}) \geq (\phi^T \Delta_t) F_{i,j} 2 q_{i,j,t} \breve{q}_{i,j,t} + (\phi^T \Delta_t)^2 F_{i,j} \breve{q}^2_{i,j,t} \quad (i,j) \in \mathcal{E}, t \in \mathcal{T} \tag{27}$$

$$\breve{h}_{i,t} - \breve{h}_{j,t} \leq r^1_{i,j} \breve{q}_{i,j,t} \quad (i,j) \in \mathcal{E}, t \in \mathcal{T}. \tag{28}$$

Parameters $r^0_{i,j}$ and $r^1_{i,j}$ denote the y-intercept and slope of the linear function, respectively. Notably, inequality (27) introduces new bilinear and quadratic terms. To enhance the convexity of (27), a novel hybrid method is proposed. This approach combines a McCormick relaxation technique applied to the bilinear term $q_{i,j,t}\breve{q}_{i,j,t}$ and a Second-Order Cone (SOC) relaxation applied to the quadratic term $\breve{q}^2_{i,j,t}$. In this context, we define the following parameters: $q^L_{i,j,t}$ and $\breve{q}^L_{i,j,t}$ represent the estimated lower bounds of variables $q_{i,j,t}$ and $\breve{q}_{i,j,t}$ respectively; $q^U_{i,j,t}$ and $\breve{q}^U_{i,j,t}$ represent the estimated upper bounds of variables $q_{i,j,t}$ and $\breve{q}_{i,j,t}$ respectively. The auxiliary variable $m_{i,j,t}$ describes the McCormick envelope. To simplify the quadratic term, we replace $\breve{q}^2_{i,j,t}$ with the auxiliary variable $\zeta^s_{i,j,t}$ and introduce one additional Second Order Cone (SOC) constraint (32). This reformulation results in a tractable representation of constraint (27) for $(i,j) \in \mathcal{E}, t \in \mathcal{T}$ as follows:

$$\phi^T \Delta_t (\breve{h}_{i,t} - \breve{h}_{j,t}) \geq (\phi^T \Delta_t) F_{i,j} 2 m_{i,j,t} + (\phi^T \Delta_t)^2 F_{i,j} \gamma_{i,j,t} \tag{29}$$

$$m_{i,j,t} \geq max\{(q^L_{i,j,t}\breve{q}_{i,j,t} + q_{i,j,t}\breve{q}^L_{i,j,t} - q^L_{i,j,t}\breve{q}^L_{i,j,t}), (q^U_{i,j,t}\breve{q}_{i,j,t} + q_{i,j,t}\breve{q}^U_{i,j,t} - q^U_{i,j,t}\breve{q}^U_{i,j,t}\} \tag{30}$$

$$m_{i,j,t} \leq min\{(q^U_{i,j,t}\breve{q}_{i,j,t} + q_{i,j,t}\breve{q}^L_{i,j,t} - q^U_{i,j,t}\breve{q}^L_{i,j,t}), (q^L_{i,j,t}\breve{q}_{i,j,t} + q_{i,j,t}\breve{q}^U_{i,j,t} - q^L_{i,j,t}\breve{q}^U_{i,j,t})\} \tag{31}$$

$$\breve{q}^2_{i,j,t} \leq \zeta^s_{i,j,t}. \tag{32}$$

Next, we focus on approximating the pump hydraulic curve (7). Variable speed pumps are commonly characterized by quadratic functions of the flow rate, representing the pressure head gain of pump (i,j) at time t. Constraint (7) poses computational challenges as it is nonlinear and non-convex. Moreover, the hydraulic behaviour of a variable-speed pump is significantly affected by its operating speed. The first pump affinity law states that the flow rate of a pump is directly proportional to its rotational speed, while the head it generates is proportional to the square of the rotational speed. Consequently, a factor denoted as $\underline{\aleph}_{i,j,t} \leq \aleph_{i,j,t} \leq \overline{\aleph}_{i,j,t}$ is used to adjust the hydraulic curve as follows: $\tilde{h}_j - \tilde{h}_i = a_{i,j}\tilde{q}^2_{i,j} + \aleph_{i,j,t} b_{i,j} \tilde{q}_{i,j} + \aleph^2_{i,j,t} c_{i,j}$. Here, $\aleph_{i,j,t}$ is the relative speed, defined as the ratio between the actual operational speed and the nominal pump speed. Parameters $\underline{\aleph}_{i,j,t}$ and $\overline{\aleph}_{i,j,t}$ correspond to the lower and upper bounds of this ratio, establishing the feasible pump operating region. Adopting a comparable strategy as in [29] and [30], the upper and lower pump's hydraulic functions are approximated through a linear model such that $\underline{\aleph}^2_{i,j,t} c_{i,j} + \underline{\aleph}_{i,j,t} b'_{i,j} \tilde{q}_{i,j} \leq \tilde{h}_j - \tilde{h}_i \leq \overline{\aleph}^2_{i,j,t} c_{i,j} + \overline{\aleph}_{i,j,t} b'_{i,j} \tilde{q}_{i,j}$ as shown in Figure 2b. By expanding the linear pump's hydraulic functions to both their nominal and uncertainty-dependent parts, we derive constraints (33)-(36) as follows:

$$h_{j,t} - h_{i,t} \leq \overline{\aleph}^2_{i,j,t} c'_{i,j} + \overline{\aleph}_{i,j,t} b'_{i,j} q_{i,j,t} \quad (i,j) \in \mathcal{P}, t \in \mathcal{T} \tag{33}$$

$$h_{j,t} - h_{i,t} \geq \underline{\aleph}^2_{i,j,t} c'_{i,j} + \underline{\aleph}_{i,j,t} b'_{i,j} q_{i,j,t} \quad (i,j) \in \mathcal{P}, t \in \mathcal{T} \tag{34}$$

$$h_{j,t} - h_{i,t} + \phi^T \Delta_t (\breve{h}_{j,t} - \breve{h}_{i,t}) \leq \overline{\aleph}^2_{i,j,t} c'_{i,j} + \overline{\aleph}_{i,j,t} b'_{i,j} (q_{i,j,t} + \phi^T \Delta_t \breve{q}_{i,j,t}) \quad (i,j) \in \mathcal{P}, t \in \mathcal{T} \tag{35}$$

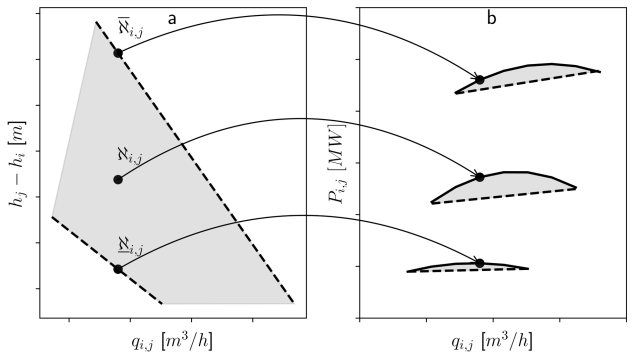

FIGURE 3. Convex approximations of pump power consumption. (a) The feasible hydraulic region with three operating points at different speeds and fixed flow rate. (b) Convex approximation of energy consumption curve for the three different operating speeds: real power curve (solid), linear cut (dashed), feasible region (grey).

$$h_{j,t} - h_{i,t} + \phi^T \Delta_t(\check{h}_{j,t} - \check{h}_{i,t}) \geq \underline{\aleph}^2_{i,j,t} c'_{i,j} + \underline{\aleph}_{i,j,t} b'_{i,j}(q_{i,j,t} + \phi^T \Delta_t \check{q}_{i,j,t}) \quad (i,j) \in \mathcal{P}, t \in \mathcal{T}. \tag{36}$$

The values of $b'_{i,j}$, $c'_{i,j}$, $\overline{\aleph}_{i,j,t}$, and $\underline{\aleph}_{i,j,t}$ are reliant on the distinctive attributes of the chosen water pump (i,j) and can be computed based on pump characteristic curves and technical data sheets.

Next, we focus on approximating the pump power consumption expression. The power needed to operate the electric motor of a variable-speed pump is modelled as a function of pump flow and pressure head gain, as given in equation (8), which is non-convex. Further, it is known that the power required by a variable speed pump is proportional to the cube of the pump operating speed. Let us consider a variable speed pump which must deliver a specific water flow $q_{i,j}$ to the system. Depending on the pump operating speed, this flow can be supplied at different pressures $(h_j - h_i)$ as shown in Figure 3a.

For known pump operating speed, equation (8) can be expressed as a concave quadratic function of the flow rate of the form $\tilde{P}_{i,j,t} = \aleph_{i,j,t} x_{i,j} \tilde{q}^2_{i,j,t} + \aleph^2_{i,j,t} y_{i,j} \tilde{q}_{i,j,t} + \aleph^3_{i,j,t} z_{i,j}$. Following the convex hull relaxation approach as above, this is modelled as the intersection of a concave function and a linear function such that $\aleph^2_{i,j,t} y'_{i,j} \tilde{q}_{i,j,t} + \aleph^3_{i,j,t} z'_{i,j} \leq \tilde{P}_{i,j,t} \leq \aleph_{i,j,t} x_{i,j} \tilde{q}^2_{i,j,t} + \aleph^2_{i,j,t} y_{i,j} \tilde{q}_{i,j,t} + \aleph^3_{i,j,t} z_{i,j}$ as shown in Figure 3b. By expanding this expression to describe both uncertainty-dependent and independent terms, we obtain constraints (37)-(40) as follows:

$$P_{i,j,t} \leq \aleph_{i,j,t} x_{i,j} q^2_{i,j,t} + \aleph^2_{i,j,t} y_{i,j} q_{i,j,t} + \aleph^3_{i,j,t} z_{i,j} \quad (i,j) \in \mathcal{P}, t \in \mathcal{T} \tag{37}$$

$$P_{i,j,t} \geq \aleph^2_{i,j,t} y'_{i,j} q_{i,j,t} + \aleph^3_{i,j,t} z'_{i,j} \quad (i,j) \in \mathcal{P}, t \in \mathcal{T} \tag{38}$$

$$\check{P}_{i,j,t} \leq \check{\aleph}_{i,j,t} 2 x_{i,j} \check{q}_{i,j,t} q_{i,j,t} + (\phi^T \Delta_t) \check{\aleph}_{i,j,t} x_{i,j} \check{q}^2_{i,j,t} + \check{\aleph}^2_{i,j,t} y_{i,j} \check{q}_{i,j,t} \quad (i,j) \in \mathcal{P}, t \in \mathcal{T} \tag{39}$$

$$\check{P}_{i,j,t} \geq \check{\aleph}^2_{i,j,t} y'_{i,j} \check{q}_{i,j,t} \quad (i,j) \in \mathcal{P}, t \in \mathcal{T}. \tag{40}$$

The empirical parameters $x_{i,j}$, $y_{i,j}$, $y'_{i,j}$, $z_{i,j}$, $z'_{i,j}$, associated with water pump (i,j), are determined from technical data sheets, leveraging the specific attributes of the pump. Factor $\check{\aleph}_{i,j,t}$ denotes the ratio between the uncertainty-dependent operational speed and the nominal pump speed. It is evident that constraint (39) involves bilinear and quadratic components and is therefore still non-convex. Extending the novel hybrid methodology outlined above, McCormick relaxation is employed to linearize the bilinear term $q_{i,j,t} \check{q}_{i,j,t}$. The quadratic term $\check{q}^2_{i,j,t}$ is approximated using SOC relaxation, resulting in a convex representation of constraint (39) for $(i,j) \in \mathcal{P}, t \in \mathcal{T}$ as follows:

$$\check{P}_{i,j,t} \leq \check{\aleph}_{i,j,t} 2 x_{i,j} m_{i,j,t} + (\phi^T \Delta_t) \check{\aleph}_{i,j,t} x_{i,j} \zeta_{i,j,t} + \check{\aleph}^2_{i,j,t} y_{i,j} \check{q}_{i,j,t} \tag{41}$$

$$m_{i,j,t} \geq max\{(q^L_{i,j,t} \check{q}_{i,j,t} + q_{i,j,t} \check{q}^L_{i,j,t} - q^L_{i,j,t} \check{q}^L_{i,j,t}), (q^U_{i,j,t} \check{q}_{i,j,t} + q_{i,j,t} \check{q}^U_{i,j,t} - q^U_{i,j,t} \check{q}^U_{i,j,t})\} \tag{42}$$

$$m_{i,j,t} \leq min\{(q^U_{i,j,t} \check{q}_{i,j,t} + q_{i,j,t} \check{q}^L_{i,j,t} - q^U_{i,j,t} \check{q}^L_{i,j,t}), (q^L_{i,j,t} \check{q}_{i,j,t} + q_{i,j,t} \check{q}^U_{i,j,t} - q^L_{i,j,t} \check{q}^U_{i,j,t})\} \tag{43}$$

$$\check{q}^2_{i,j,t} \leq \zeta^p_{i,j,t}. \tag{44}$$

Parameters $q^L_{i,j,t}$, $\check{q}^L_{i,j,t}$, $q^U_{i,j,t}$ and $\check{q}^U_{i,j,t}$ represent the estimated upper and lower bounds of variables $q_{i,j,t}$ and $\check{q}_{i,j,t}$ respectively; $m_{i,j,t}$ and $\zeta^p_{i,j,t}$ serve as auxiliary variables within the McCormick relaxation and SOC relaxation, respectively.

III. SOLUTION APPROACH

A. DRCC PROGRAM REFORMULATION

The complete reformulation of the program is presented herein, assuming an affine response to uncertainty and utilizing the analytical reformulation of DRCCs and the convex relaxations and approximations outlined in Section II-C and II-D. Under the assumption of zero mean forecast error, the optimisation problem simplifies to a minimization problem. This is because, within the ambiguity set, any probability distribution will lead to the same worst-case expectation. Therefore, the worst-case distribution is determined solely by its covariance. The reformulated DRCC problem takes the following form.

$$\underset{\Xi, \mathbb{P} \in \Pi}{Min} \sum_{t \in \mathcal{T}} \left[\left(\sum_{e \in \mathcal{G}} C^G_e(p^G_{e,t}) - \sum_{l \in \mathcal{D}} U^D_l p^D_{l,t} - \sum_{u \in \mathcal{P}} U^P_u p^P_{u,t} \right) + \sum_{e \in \mathcal{G}} C^{Av}_e \alpha_{e,t} + \sum_{u \in \psi_P} C^{Av}_u \beta_{u,t} \right] \tag{45}$$

$$s.t.\ \check{h}_{r,t} = 0 \; r \in \mathcal{R}, t \in \mathcal{T} \tag{46}$$

$$\sum_{i \in N_{in} J} \check{q}_{i,j,t} - \sum_{k \in N_{out} J} \check{q}_{j,k,t} = 0 \; j \in \mathcal{J}, t \in \mathcal{T} \tag{47}$$

$$\check{h}_{s,t} = \frac{\tau}{A_s} \left(\sum_{i \in N_{in} s} \check{q}_{i,s,t} - \sum_{j \in N_{out} s} \check{q}_{s,j,t} \right) s \in \mathcal{S}, t = 1 \tag{48}$$

$$\breve{h}_{s,t} - \breve{h}_{s,t-1} = \frac{\tau}{A_s}\left(\sum_{i\in N_{in}s} \breve{q}_{i,s,t} - \sum_{j\in N_{out}s} \breve{q}_{s,j,t}\right)$$
$$s \in \mathcal{S}, t > 1 \quad (49)$$

$$\breve{h}_{j,t} - \breve{h}_{i,t} \geq F_{i,j} 2 m_{i,j,t} + \epsilon' \gamma_t F_{i,j} \zeta^s_{i,j,t} \; (i,j) \in \mathcal{E}, t \in \mathcal{T} \quad (50)$$

$$h_{j,t} - h_{i,t} + \epsilon' \gamma_t (\breve{h}_{j,t} - \breve{h}_{i,t}) \leq \overline{\aleph}^2_{i,j,t} c_{i,j} - \overline{\aleph}_{i,j,t} b'_{i,j} (q_{i,j,t} + \epsilon' \gamma_t \breve{q}_{i,j,t}) \; (i,j) \in \mathcal{P}, t \in \mathcal{T} \quad (51)$$

$$h_{j,t} - h_{i,t} + \epsilon' \gamma_t (\breve{h}_{j,t} - \breve{h}_{i,t}) \geq \underline{\aleph}^2_{i,j,t} c_{i,j} - \underline{\aleph}_{i,j,t} b'_{i,j} (q_{i,j,t} + \epsilon' \gamma_t \breve{q}_{i,j,t}) \; (i,j) \in \mathcal{P}, t \in \mathcal{T} \quad (52)$$

$$\breve{P}_{i,j,t} \leq \breve{\aleph}_{i,j,t} 2 x_{i,j} m_{i,j,t} + \epsilon' \gamma_t \aleph_{i,j,t} x_{i,j} \zeta_{i,j,t} + \breve{\aleph}^2_{i,j,t} y_{i,j} \breve{q}_{i,j,t} \; (i,j) \in \mathcal{P}, t \in \mathcal{T} \quad (53)$$

$$\underline{H}_j + H^0_j \leq h_{j,t} \leq \overline{H}_j + H^0_j \; j \in (\mathcal{J} \cup \mathcal{S}), t \in \mathcal{T} \quad (54)$$

$$\underline{H}^{end}_s \leq h_{s,t} \leq \overline{H}^{end}_s \; s \in \mathcal{S}, t = end \quad (55)$$

$$\underline{Q}_{i,j} \leq q_{i,j,t} \leq \overline{Q}_{i,j} \; (i,j) \in (\mathcal{E} \cup \mathcal{P}), t \in \mathcal{T} \quad (56)$$

$$\epsilon' \gamma_t \breve{h}_{j,t} \geq -h_{j,t} + \underline{H}_j + H^0_j \; j \in (\mathcal{J} \cup \mathcal{S}), t \in \mathcal{T} \quad (57)$$

$$\epsilon' \gamma_t \breve{h}_{j,t} \leq -h_{j,t} + \overline{H}_j + H^0_j \; j \in (\mathcal{J} \cup \mathcal{S}), t \in \mathcal{T} \quad (58)$$

$$\epsilon' \gamma_t \breve{h}_{s,t} \geq -h_{s,t} + \underline{H}^{end}_s \; s \in \mathcal{S}, t = end \quad (59)$$

$$\epsilon' \gamma_t \breve{h}_{s,t} \leq h_{s,t} + \overline{H}^{end}_s \; s \in \mathcal{S}, t = end \quad (60)$$

$$\sum_{e\in\mathcal{G}} \breve{p}^G_{e,t} - \sum_{u\in\mathcal{P}} \breve{p}^P_{u,t} = 1 \; t \in \mathcal{T} \quad (61)$$

$$\sum_{e\in\psi_{Gn}} \breve{p}^G_{e,t} - \sum_{u\in\psi_{Pn}} \breve{p}^P_{u,t} - \sum_{m\in\Omega n} \breve{f}_{n,m,t} = 0 \; n \in \mathcal{N}, t \in \mathcal{T} \quad (62)$$

$$\underline{P}^G_e \leq p^G_{e,t} \leq \overline{P}^G_e \; e \in \mathcal{G}, t \in \mathcal{T} \quad (63)$$

$$p^G_{e,t} + \epsilon' \gamma_t \breve{p}^G_{e,t} \leq \overline{P}^G_e \; e \in \mathcal{G}, t \in \mathcal{T} \quad (64)$$

$$p^G_{e,t} + \epsilon' \gamma_t \breve{p}^G_{e,t} \geq \underline{P}^G_e \; e \in \mathcal{G}, t \in \mathcal{T} \quad (65)$$

$$\underline{f}_{n,m} \leq f_{n,m,t} \leq \overline{f}_{n,m} \; (n,m) \in \mathcal{L}, t \in \mathcal{T} \quad (66)$$

$$f_{n,m,t} + \epsilon' \gamma_t [E^2_0 B_{n,m} (\breve{\theta}_{n,t} - \breve{\theta}_{m,t})] \leq \overline{f}_{n,m} \; (n,m) \in \mathcal{L}, t \in \mathcal{T} \quad (67)$$

$$f_{n,m,t} + \epsilon' \gamma_t [E^2_0 B_{n,m} (\breve{\theta}_{n,t} - \breve{\theta}_{m,t})] \geq \underline{f}_{n,m} \; (n,m) \in \mathcal{L}, t \in \mathcal{T} \quad (68)$$

$$\breve{\theta}_{n,t} = 0 \; n = ref, t \in \mathcal{T} \quad (69)$$

$$\breve{p}^P_{u,t} = \breve{P}_{i,j,t} + \delta_{i,j,t} \breve{q}_{i,j,t} \; u \in \psi_{P_{i,j}}, (i,j) \in \mathcal{P}, t \in \mathcal{T} \quad (70)$$

$$\alpha_{e,t} \geq \left\| \breve{p}_{e,t} \Sigma^{1/2}_t \right\|_2 \; e \in \mathcal{G}, t \in \mathcal{T} \quad (71)$$

$$\beta_{u,t} \geq \left\| \breve{p}^P_{u,t} \Sigma^{1/2}_t \right\|_2 \; u \in \psi_P, t \in \mathcal{T} \quad (72)$$

$$(2)-(5), (14)-(19), (23)-(26), (28) \; (30)-(34), (37), (38), (40), (42)-(44) \quad (73)$$

Here $\Xi = p^D_{l,t}, p^G_{e,t}, \breve{p}^G_{e,t}, p^W_{w,t}, p^P_{u,t}, \breve{p}^P_{u,t}, \theta_{n,t}, \breve{\theta}_{n,t}, f_{n,m,t}, \breve{f}_{n,m,t}, h_{i,t}, \breve{h}_{i,t}, h_{r,t}, q_{i,j,t}, \breve{q}_{i,j,t}, h_{s,t}, \breve{h}_{s,t}, P_{i,j,t}, \breve{P}_{i,j,t}, m_{i,j,t}, \zeta^s_{i,j,t}, \zeta^p_{i,j,t}, \alpha_{e,t}, \beta_{u,t}$ is the set of nominal and uncertainty-dependent optimisation decision variables. In (45), C^{Av}_e is the availability cost for flexible generators and C^{Av}_u for pumps. Availability cost refers to the expense incurred by the market operator to make sure that flexible generators or pumps are prepared to adjust their operations near RT. In this research, we assume that the availability cost serves as the sole pricing mechanism governing deploying flexibility. As such, it represents the main source of income for flexible generators and water pumps during RT operations. Introducing availability costs results in an augmented DA market clearing problem, in which the cost of flexibility utilization in RT is externalized from the DA social welfare. Variable $\alpha_{e,t}$ and $\beta_{u,t}$ represent the absolute amount of flexibility offered by generators e and pumps u at time t, respectively. Notably, constraint (47) ensures that uncertainty-dependent water flow differences must be equal to zero. Constraints (61) and (62) ensure that under uncertainty, total RES mismatches are fully compensated, and changes in generation and pump load at a node must match changes in power flow across connected lines. Constraint (70) sets the uncertainty-dependent pump power load on the PN equal to the uncertainty-dependent pump power consumption plus a correction factor $\delta_{i,j,t} \breve{q}_{i,j,t}$. Constraints (71) and (72) enforce that the absolute amount of flexibility offered by generators and pumps must be larger or equal to the L2-Norm of the vector of uncertainty-dependent generation and pump power load multiplied by the square root of the covariance matrix.

B. ITERATIVE SOLUTION ALGORITHM

Assuming known DA and RT pump operating speeds, program (45)-(73) is convex and therefore computationally tractable. However, the optimal pump operating speed is currently unknown and must be determined through optimisation. We propose to solve the convex optimisation problem iteratively, by adjusting the pump relative speed $\aleph_{i,j,t}$ and $\breve{\aleph}_{i,j,t}$ until a predefined termination condition is met. The proposed algorithm leverages known pump properties and affinity laws with the convex relaxation and approximations developed in this study. Algorithm 1 summarizes the overall solution procedure. The algorithm begins by initializing the iteration counter (it), the objective value placeholder (obj^{it-1}) and arrays $\aleph$, $\breve{\aleph}$, and δ of dimensions $\mathcal{P}, \mathcal{T}$. Within each iteration, it solves program (45)-(73) to determine decision vectors q, $\breve{q}$, h, $\breve{q}$. For each time step t and pump i,j, it computes the values of $\Delta h^{ref,DA}$, Δh^{DA}, $\Delta h^{ref,RT}$, and Δh^{RT} representing the reference and actual pressure head gain in DA and RT, respectively. The relative pump operating speed in DA ($\aleph_{i,j,t}$), and RT ($\breve{\aleph}_{i,j,t}$) is calculated based on pump affinity laws. The relative speeds are used to update the pump hydraulic feasibility cuts (37), (38), (40) and (53) in the next iteration. The factor $\delta_{i,j,t}$ is used to map the estimated pressure head gain to the minimum change in pump power consumption in RT in (70). Then, the algorithm checks for convergence based on the relative percentage difference in the objective value (obj) compared to the previous iteration (obj^{it-1}). If the percentage difference

Algorithm 1 Iterative Solution of DRCC Program

$it \leftarrow 0$
$obj^{it-1} \leftarrow 0$
Initialize arrays: $\aleph$, $\breve{\aleph}$ and δ of size $(\mathcal{P}, \mathcal{T})$
while true **do**
  Solve (45)-(73):
  obj, q, $\breve{q}$, h, $\breve{q} \leftarrow$ solution of (45)-(73)
  for t in $\mathcal{T}$ **do**
    for i, j in $\mathcal{P}$ **do**
      $\Delta h^{ref,DA} \leftarrow b'_{i,j} \cdot q_{i,j,t} + c'_{i,j}$
      $\Delta h^{DA} \leftarrow h_{j,t} - h_{i,t}$
      $\Delta h^{ref,RT} \leftarrow b'_{i,j}(q_{i,j,t} + \Sigma_t^{1/2} \cdot \breve{q}_{i,j,t}) + c'_{i,j}$
      $\Delta h^{RT} \leftarrow h_{j,t} - h_{i,t} + \Sigma_t^{1/2}(\breve{h}_{j,t} - \breve{h}_{i,t})$
      $\aleph_{i,j,t} \leftarrow \sqrt{\frac{\Delta h^{DA}}{\Delta h^{ref,DA}}}$
      $\breve{\aleph}_{i,j,t} \leftarrow \sqrt{\frac{\Delta h^{RT}}{\Delta h^{ref,RT}}}$
      $\delta_{i,j,t} \leftarrow \frac{g\rho\tau}{\eta_{i,j}} \Delta h^{RT}$
    end for
  end for
  if $\frac{|obj^{it-1} - obj|}{\frac{|obj^{it-1}| + |obj|}{2}} \cdot 100 \leq \Upsilon$ **then**
    Break: Optimal solution found
  end if
  $it \leftarrow it + 1$
  $obj^{it-1} \leftarrow obj$
end while

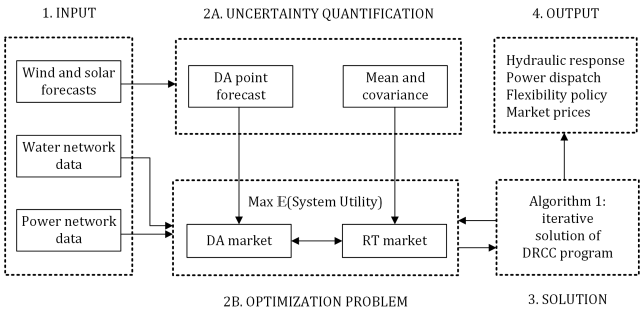

FIGURE 4. Schematic overview of the proposed coordination mechanism.

is below a given threshold (Υ), the algorithm terminates, leading to the solution of the DRCC program.

C. SOFTWARE DESCRIPTION

The general overview of the coordination mechanism and the internal process of the software is shown in Figure 4. The model requires input data including hourly solar and wind power generation forecasts, along with representative infrastructure data for water and power networks. This includes details of the pressurised water system such as network topology, reservoirs, tanks, consumption nodes, water demand profile and pipeline parameters. PN data includes network topology, generation capacity, load profile, power line parameters, and market-related factors such as

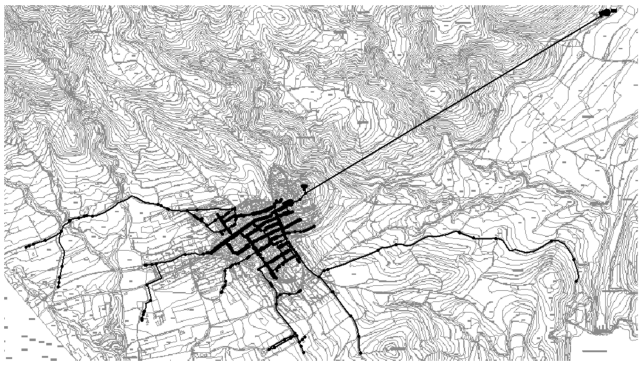

FIGURE 5. Top view of the municipality highlighting the complete water distribution network.

bidding curves. Uncertainty is quantified using a set of imperfect solar and wind power forecasts. Based on observed forecast errors, mean and covariance are computed for the next day and used to build the ambiguity set for the DRCC program. Utilizing the collected data, the DRCC program is solved iteratively via Algorithm 1. The objective function maximizes social welfare while reserving enough flexibility in the network to compensate for possible power imbalances in RT resulting from the worst-case uncertainty realization. The results provide insights into hydraulic response, power dispatch, flexibility allocation policies, and Market Clearing Prices (MCPs).

IV. CASE STUDY

We illustrate the applicability of our approach through a case study in Spain, specifically focused on a real WN located in Alicante Province within the South-Eastern region. The population is 1270 inhabitants supplied by 900 connections. The network spans 14.61 km of pipes, with 9.5% having diameters below 60 mm and 90.5% ranging from 60 to 150 mm. The pipe composition includes fibre cement (38.2%), PVC (13.0%), and polyethylene (48.8%). The infrastructure comprises a reservoir at an elevation of 293 m and a compensation tank with a diameter of 13.4 m located at an elevation of 432.31 m. The tank's water level fluctuates between 0.5 and 3.9 m. The network layout is presented in Figure 5.

The municipality's daily consumption stands at 718.54 m^3, and no leakage is accounted for in this model. Furthermore, adhering to the conditions of our problem, there are no instances of unsupplied demands within the municipality (amounting to 0%). Pump energy consumption is 264.15 kWh/day, while the reservoir contributes 535.75 kWh/day. Both total user demand and hourly modulation coefficients remain constant throughout the year. In our model, we simplify the network by excluding municipal pipes located downstream of the compensation tank, leaving five nodes connected by four main pipes. As the downstream connections are gravity-fed, this simplification does not impact the system's hydraulic behaviour. The PN is based on

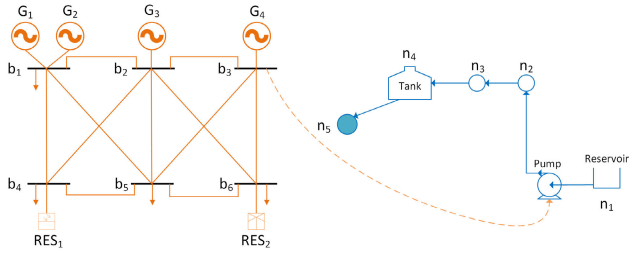

FIGURE 6. Power network (left) and water network (right) depicting orange lines as power lines, black bars as power buses, conventional and renewable generators with respective icons, blue arrows as water pipes, empty blue dots as junctions, filled blue dots as water demand points, and reservoir, tank, and pump with respective icons.

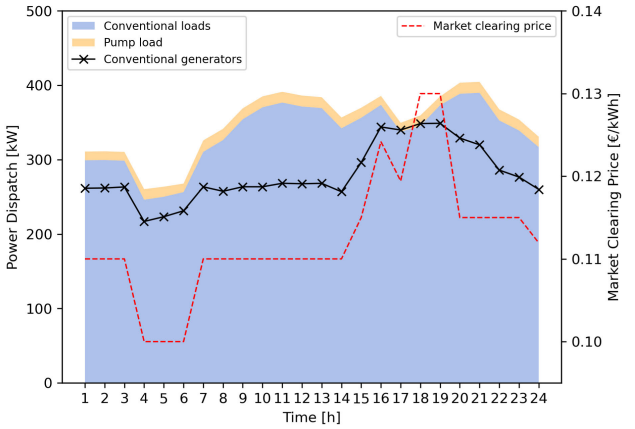

FIGURE 7. Scheduled DA power dispatch: conventional power loads (blue area), pump loads (yellow area), conventional generation (black line), and market clearing price (red dashed line).

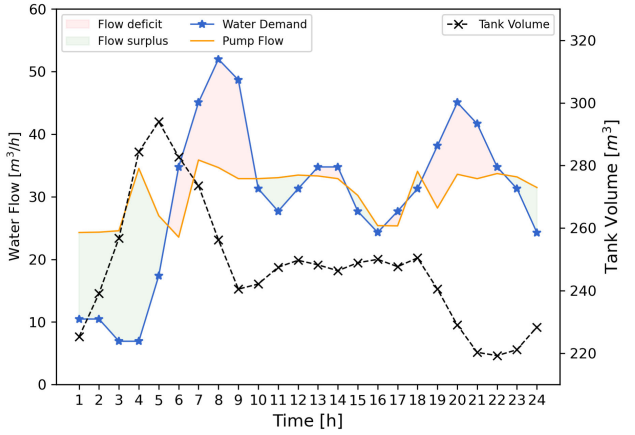

FIGURE 8. Scheduled DA water flows: water demand (blue line), pump flow (yellow line), tank volume (black dashed line), flow surplus (green area) and flow deficit (orange area).

a modified 6-Bus System introduced in [47]. It incorporates four conventional generators, one small wind turbine with a maximum power output of 150 kW, and a community solar farm with a maximum power output of 100 kW. The network comprises four conventional loads and one pump load with a maximum power requirement of 50 kW. Different nodes are connected through 11 power lines, with the reference bus situated at node 5. An overview of the coupled power and water network is given in Figure 6. A set of 1000 wind and 1000 solar forecast scenarios is used to estimate the covariance matrix of wind and solar forecast errors, following the methodology in [37]. The violation probability ϵ is fixed at a value of 0.25 for all DRCCs. The availability cost is set to 0.05 €/KW for conventional generators (i.e., C_e^{Av}) and 0.005 €/kW for water pumps (i.e., C_u^{Av}).

V. RESULTS AND DISCUSSION

All simulations are implemented in Julia v1.5.3, modelled with JuMP v0.21.6, and solved with Mosek v1.2.1. The problem is solved with an average CPU time of 0.27 seconds and 6 iterations, using a laptop with 32GB RAM with a Processor Intel(R) Xeon(R) 6 Core(s) running at 2.80GHz.

A. NUMERICAL RESULTS

The results show how the power and water network would respond to different schedules and probabilities. The optimised DA power dispatch schedule is shown in Figure 7, achieved by coordinating power and water networks.

Results show that aggregate load varies throughout the day with two major peaks around noon and in the evening around 8 PM. A significant portion of the load is fulfilled by conventional generators, with the remaining fraction sourced from wind and solar. RES generation is subject to fluctuations across the 24-hour span, with a relatively larger share of RES available between 9 AM and 2 PM as well as between 8 PM and 12 PM. The pump load constitutes a small percentage of the overall load and remains comparably constant throughout the day. The MCPs, calculated through the dual variable associated with the power balance constraint (16), vary between a minimum of 0.10 €/KWh between 4 and 6 AM, and a maximum of 0.13 €/KWh between 6 and 7 PM. Changes in MCP are driven by the bidding parameters, the availability of RES, and the aggregated load on the PN.

Figure 8 presents the DA schedule for the WN. The water demand exhibits significant variations throughout the day, with a minimum of 8 m^3/h between 3 and 4 AM, and a maximum of 52 m^3/h at 8 AM. The pump supplies water to the system, while the water flow fluctuates between 25 m^3/h (1 - 3 AM) and 36 m^3/h (7 AM). During specific intervals, the pump provides more water than the actual municipal demand, leading to a surplus of water that is stored in the compensation tank. Consequently, the tank's volume increases. Conversely, when the pumps supply less water than demanded, a deficit arises, causing the sourcing of water from the tank, which results in diminishing the tank's volume. The storage tank's volume varies between a maximum of 300 m^3 at 5 AM and a minimum of approximately 222 m^3 at 10 PM, remaining within the feasible limits defined by the specific tank dimensions. The dynamic fluctuations in tank volume show

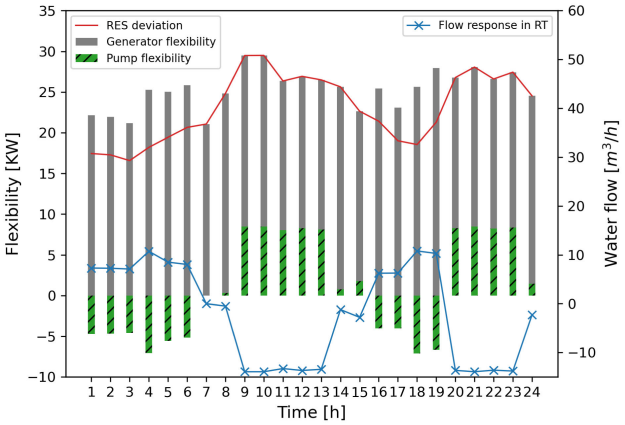

FIGURE 9. Allocation of flexibility reserves: conventional generators (grey) and water pumps (green) are assigned flexibility reserves. The red line represents the worst-case RES deviation in RT, while the blue line illustrates the dynamic pump flow adjustments in response to uncertainty.

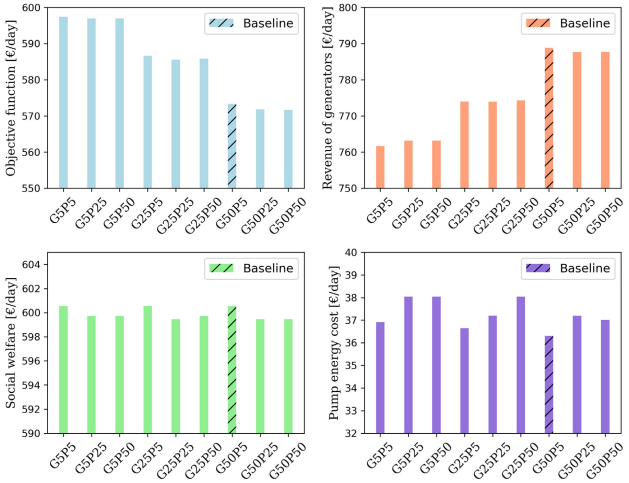

FIGURE 10. Model sensitivity across scenarios with varied availability costs.

a negative correlation with MCPs. When MCPs are low, the storage tank volume is high, and vice versa. This trend aligns with instances of a comparatively low aggregated load on the PN and high availability of RES. These findings underscore the effectiveness of smart water system operation in its capacity as a DR provider, emphasizing its potential to enhance economic efficiency.

Next to the DA schedule, flexible generators and water pumps are assigned dynamic flexibility policies during the RT stage. These policies compensate for unforeseen RES deviations under worst-case conditions. This ensures enough flexibility reserves, necessary for maintaining stability in both power and water networks during RT. As depicted in Figure 9, the distribution of these flexibility reserves is illustrated with generators shown in grey and pumps in green. The heights of the bars show the size of flexibility contributed to each asset. Positive generation reserves denote increased power production, while positive pump reserves signify curtailed power consumption. The aggregate flexibility from generators and pumps must align with the RES power deviation depicted by the red line. This ensures a complete compensation of power deviations. Results show that generators contribute a substantial portion of the RES deviation, ranging from 73% (9 AM - 1 PM) to 100% of the total RES mismatch from 1 to 7 AM and 4 to 7 PM. Pump-driven flexibility, constrained by pump size and hydraulic limitations, is comparatively lower, but still significant. From 1 to 6 AM and 4 to 7 PM, the water pump increases its flow (blue line), consequently increasing energy consumption. Conversely, from 9 AM to 1 PM and 8 to 12 PM, the pump reduces its flow and thus, its power consumption. These outcomes unveil a time-sensitive bidirectional response pattern in water pumps. Logically, during the time intervals of 1 to 6 AM and 4 to 7 PM, the increased water flow results in additional water being stored in the compensation tank. This surplus water is subsequently used to enable load reduction by the pump during alternate periods. This mechanism enables the water system to adapt its operations, providing RT flexibility while maintaining the security of the water supply.

B. SENSITIVITY ANALYSIS

To gain deeper insight into the model's behaviour, a one-factor-at-a-time sensitivity analysis is conducted. We examine the influence of altering different parameters on the optimal solution. Specifically, the analysis focuses on varying availability costs, varying constraint violation probability level ϵ, and varying hydraulic conditions. Figure 10 illustrates the model's sensitivity to varying availability costs (i.e., C_e^{Av} for flexible generators and C_u^{Av} for pumps) ranging from 0.005 to 0.05 €/KW. For instance, in scenario G5P50, the availability cost is 0.005 €/KW for generators (G) and 0.05 €/KW for pumps (P). The model is evaluated across multiple metrics: objective function value (upper left), social welfare (lower left), generator revenue (upper right), and pump energy cost (lower right). Results show a reduction in the objective function value as the availability costs of flexible generators increase. Social welfare, defined as the difference between the benefit of consumption and the cost of production, maintains a constant pattern across all scenarios. Nevertheless, it shows a higher value in scenarios G5P5, G25P5, and G50P5. Generator revenue, defined as the sum of the revenue from DA electricity sales and RT flexibility services, displays a positive correlation with increasing generator availability costs. This suggests that generators are required to engage in RT flexibility services under all scenarios, indicating that the flexibility capacity of water pumps alone is insufficient to compensate for the RES mismatch entirely. Finally, instances of lower pump availability costs correspond to lower pump energy expenses, defined as the cost of purchasing energy in DA minus the revenue from flexibility service in RT. This suggests potential

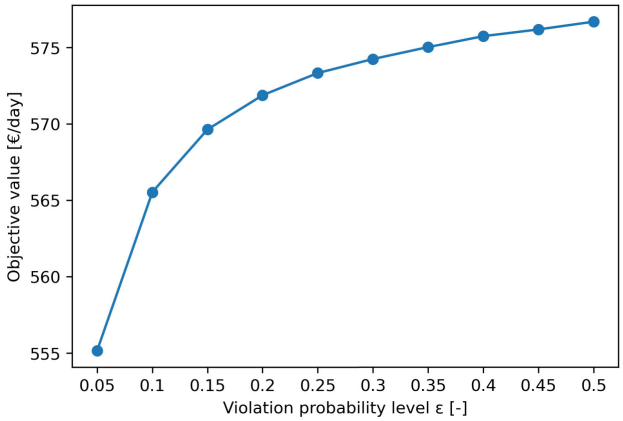

FIGURE 11. Model sensitivity to different violation probability levels.

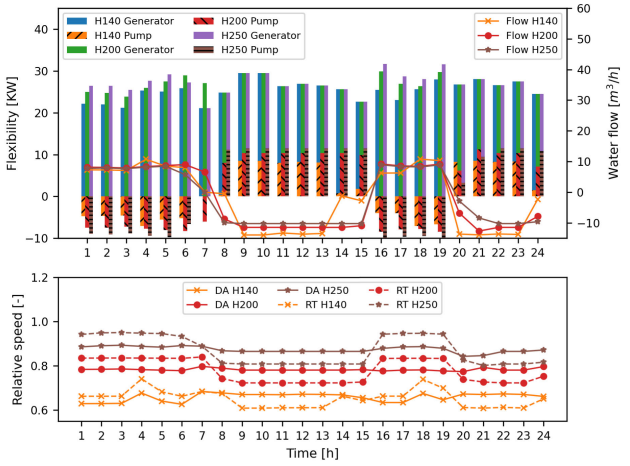

FIGURE 12. Sensitivity of Model to different Hydraulic Conditions. The top graph shows the flexibility allocation on the primary axis and the change in flow rate in RT on the secondary y-axis. The bottom graph illustrates the relative pump operating speed in DA and RT.

cost savings for the WN when providing flexibility at reduced cost rates. Though the model shows sensitivity to various availability costs, it is based on the specific economic and physical parameters of the system under study. These findings should not be generalised but approached as specific to the particular case.

Next, we examine the model sensitivity to different choices of the parameter ϵ, which determines the level of violation probability associated with CC. Figure 11 illustrates the change in the objective function value across varying values of ϵ. Notably, the objective function value increases from 555 €/day to 576 €/day as the violation probability level rises (Figure 11). This suggests that when a higher constraint violation probability is allowed, the system can incur lower costs associated with flexibility and thus achieve higher social welfare. In practice, higher constraint violation probability means that the SO has a higher degree of freedom in choosing the best schedule for the DA stage. However, this trade-off leads to a reduction in the system's confidence in dealing with uncertainty in RT, referred to as robustness. A point already established in [25] is that as one approached the maximum injected flow level into a pressurised water distribution network, the energy efficiency improved. However, this was accompanied by an increased likelihood of failing to deliver water at the specified threshold pressure (25 m) and encountering unsupplied demands. The results show the substantial impact of the parameter ϵ on the optimal solution. Therefore, its selection should be done carefully, in relation to the specific context of the application and the precise needs of the end-user.

Finally, we investigate the model sensitivity to different hydraulic heads. We define three distinct scenarios in which the static pressure head is varied. The static head is defined as the elevation difference between the reservoir and the compensation tank. The static head is progressively increased from 140 m (representing the real case) to 200 m and 250 m, denoted as scenarios H140, H200, and H250, respectively. Figure 12 shows alterations in the model response concerning flexibility provision under varying hydraulic heads (top) and shifts in relative pump operating speeds between DA and RT (bottom). The results indicate that although the flexibility provided by the generators and water pumps is affected by different hydraulic heads, the overall trend over time remains stable in all scenarios. The higher the static head, the greater the pump's flexibility. The increase in flexibility potential is because of changes in pump operating speed associated with different hydraulic heads. Relative pump speed ($\aleph_{i,j}$) increases from an average of 0.65 in scenario H140 to an average of 0.9 in scenario H250. As the pump's operating speed increases, its feasible operational range shifts vertically (see Figure 3), thereby influencing the pump's ability to adapt water flow during RT operations, and therefore its energy consumption. Results suggest that different hydraulic heads have a significant influence on the pump operating conditions and resulting capacity to deliver flexibility. Hence, selecting an appropriate variable speed pump is critical to ensuring an optimal degree of operational flexibility.

To assess the implications of implementing the second-order cone reformulation for water flows, we examine the Mean Absolute Error (MAE) resulting from the convex relaxation applied to constraints describing friction head losses in DA (25) and RT (27), as well as constraints related to pump energy consumption in DA (37) and RT (39). The MAE quantifies the slack resulting from the convex relaxations. It measures the average absolute difference between the outcomes of the original non-convex constraint and the relaxed constraint. This offers insight into the gap between the optimal solution of the non-convex problem and the solution obtained through convex relaxation. Importantly, MAE is expressed in the original units of the constraint, thereby preserving its inherent physical interpretation. The MAE is examined for different availability costs and hydraulic head scenarios as previously defined.

TABLE 1. Mean Absolute Error (MAE) introduced by second-order cone formulation of water flows under different availability costs and hydraulic heads.

Scenario	Constraints			
	25[a]	27[a]	37[b]	39[b]
G25P5	$3.01 \cdot 10^{-1}$	$5.17 \cdot 10^{-2}$	$6.32 \cdot 10^{-2}$	$2.05 \cdot 10^{-1}$
G25P25	$2.15 \cdot 10^{-1}$	$1.07 \cdot 10^{-2}$	$9.20 \cdot 10^{-4}$	$1.39 \cdot 10^{-2}$
G25P50	$2.07 \cdot 10^{-1}$	0.00	$3.12 \cdot 10^{-3}$	0.00
H140	$3.08 \cdot 10^{-1}$	$6.66 \cdot 10^{-2}$	$1.19 \cdot 10^{-1}$	$2.76 \cdot 10^{-1}$
H200	$2.17 \cdot 10^{-1}$	$8.40 \cdot 10^{-2}$	$9.60 \cdot 10^{-4}$	$3.27 \cdot 10^{-1}$
H250	$4.36 \cdot 10^{-2}$	$8.59 \cdot 10^{-2}$	$7.20 \cdot 10^{-4}$	$4.48 \cdot 10^{-1}$

[a] Values are in meters (m).
[b] Values are in kilowatts (KW).

The results, presented in Table 1, show variations in the MAE across different constraints, availability costs and hydraulic head scenarios. Notably, the MAE remains consistently low, indicating that the slack introduced by the convex relaxations stays within acceptable limits. Across varying availability cost scenarios, the MAE for all constraints decreases as the availability cost of the pump (P) increases. Conversely, when the pump provides greater flexibility due to lower availability costs, the MAE also increases, aligning with the model's assumptions. This pattern suggests that higher availability costs lead to a more accurate approximation.

Across different hydraulic head scenarios, constraints (25) and (37), which correspond to DA constraints, demonstrate a declining trend in MAE values with increasing hydraulic head. Differently, constraints (27) and (39), corresponding to RT operation, show an opposite trend. As the hydraulic head increases, the MAE increases as well. This trend is logical since a higher hydraulic head corresponds to greater pump flexibility potential, as shown in Figure 12, leading to a larger MAE in these constraints. The overall performance underscores the reliability of the employed methodology in approximating water flow constraints across various conditions. The observed low MAE values collectively indicate that the model's predictions closely match actual constraint values, thus strengthening its potential for practical applications across scenarios characterized by varying availability costs and hydraulic head settings.

C. REFLECTION

The sensitivity analysis provided valuable insights into the model's behaviour under diverse conditions. It highlighted the significant influence of flexible generator availability costs on economic performance, while the impact of pump availability costs was relatively minor. However, it's notable that water pumps offer less flexibility compared to generators due to the small scale of the water network. Expanding the water network could potentially increase flexibility and its economic impact on the power system. Exploring varying constraint violation probability levels (ϵ) revealed a trade-off between cost reduction and system robustness, similar to findings in [39] and [46]. These underscore the importance of balancing cost efficiency with system resilience by carefully considering constraint violation probabilities. Additionally, sensitivity analysis to different hydraulic conditions emphasized the influence of static pressure heads on flexibility provision and pump operations. This highlights the importance of selecting appropriate pump configurations to optimize operational flexibility under varying hydraulic conditions. Furthermore, the assessment of MAE resulting from convex relaxation indicated the reliability of the methodology in approximating non-convex constraints across various scenarios. However, these findings are specific to the system's characteristics, necessitating further analysis of different water network infrastructures for generalization.

Finally, it is worth mentioning that the scalability of the proposed approach has not been examined. However, we note that the proposed mathematical programming problem is a SOCP. One important advantage of SOCPs is their computational efficiency compared to non-convex programs. For SOCPs, the globally optimal solution can be computed in polynomial time for a wide range of problem types and sizes, as discussed in [48]. Our previous work [34] further supports this notion. We investigated a similar problem in a relatively larger system, using an IEEE 24-bus reliability test system and a water network with 20 nodes. Our results demonstrated that these types of convex problems can be solved efficiently at this scale. However, when modelling larger systems, the error introduced by convex relaxations may increase. Therefore, conducting additional analysis on even larger systems would further strengthen these findings, providing opportunities for future research.

VI. CONCLUSION

This study presents a novel market-based mechanism for the integrated scheduling of power and water networks. The model is formulated as a distribution robust chance-constrained optimisation problem. It optimises flexible resources to make up for imperfect renewable energy forecasts. The approach maximises utility in the power sector and compensates for power deviations in real-time while ensuring a stable water supply to the community. Simultaneously, it seeks to enhance the storage of water (and energy) in the head and/or compensation tanks. We introduce a novel relaxation technique to handle the non-convexity arising from the WN constraints. Further, we propose a novel iterative solution algorithm to estimate the variable speed pump behaviour. This method simplifies the study of water networks for more efficient modelling and optimisation of power and water networks. Adopting a look-ahead strategy, this approach leads to a network-aware and resilient day-ahead scheduling solution for power and water networks. Notably, the outcomes underscore the successful harnessing of WN flexibility by the power system. As such, the proposed coordination mechanism enhances the overall utility and system-wide resilience without impacting water end-users. This tool helps utility managers and practitioners plan and operate power and water networks more effectively. In future

work, we will investigate the scalability of our approach by testing it on larger power and water network sizes and finer time resolutions. Further, we aim to investigate optimal pump selection, optimal tank sizing, and integrated power and water network investment planning. Additionally, we will investigate the flexibility of other water infrastructural components, such as pumps-as-turbines (PATs) and desalination plants. Finally, we will investigate the impact of different uncertainty sources such as stochastic power loads and water demands.

REFERENCES

[1] *World Energy Outlook 2017*, IEA, 2017.
[2] A. Ramos, C. De Jonghe, V. Gómez, and R. Belmans, "Realizing the smart grid's potential: Defining local markets for flexibility," *Utilities Policy*, vol. 40, pp. 26–35, Jun. 2016.
[3] M. G. Simões, R. Roche, E. Kyriakides, S. Suryanarayanan, B. Blunier, K. D. McBee, P. H. Nguyen, P. F. Ribeiro, and A. Miraoui, "A comparison of smart grid technologies and progresses in Europe and the U.S.," *IEEE Trans. Ind. Appl.*, vol. 48, no. 4, pp. 1154–1162, Jun. 2012.
[4] *World Energy Outlook 2019*, Int. Energy Agency, 2019.
[5] V. G. Gude, "Energy and water autarky of wastewater treatment and power generation systems," *Renew. Sustain. Energy Rev.*, vol. 45, pp. 52–68, May 2015.
[6] G. Kumar and B. W. Karney, "Electricity usage in water distribution networks," in *Proc. IEEE Canada Electr. Power Conf.*, Oct. 2007, pp. 97–102.
[7] N. Melián-Martel, B. del Río-Gamero, and J. Schallenberg-Rodríguez, "Water cycle driven only by wind energy surplus: Towards 100% renewable energy islands," *Desalination*, vol. 515, Nov. 2021, Art. no. 115216.
[8] R. Heffron, M.-F. Körner, J. Wagner, M. Weibelzahl, and G. Fridgen, "Industrial demand-side flexibility: A key element of a just energy transition and industrial development," *Appl. Energy*, vol. 269, Jul. 2020, Art. no. 115026.
[9] S. S. Torbaghan, G. Suryanarayana, H. Höschle, R. D'hulst, F. Geth, C. Caerts, and D. Van Hertem, "Optimal flexibility dispatch problem using second-order cone relaxation of AC power flows," *IEEE Trans. Power Syst.*, vol. 35, no. 1, pp. 98–108, Jan. 2020.
[10] S. Shariat Torbaghan, M. Madani, P. Sels, A. Virag, H. Le Cadre, K. Kessels, and Y. Mou, "Designing day-ahead multi-carrier markets for flexibility: Models and clearing algorithms," *Appl. Energy*, vol. 285, Mar. 2021, Art. no. 116390.
[11] H. Meschede, "Increased utilisation of renewable energies through demand response in the water supply sector—A case study," *Energy*, vol. 175, pp. 810–817, May 2019.
[12] D. Sauri, "The decline of water consumption in Spanish cities: Structural and contingent factors," *Int. J. Water Resour. Develop.*, vol. 36, no. 6, pp. 909–925, Nov. 2020.
[13] J. Willet, K. Wetser, J. E. Dykstra, A. B. Bianchi, G. H. P. Oude Essink, and H. H. M. Rijnaarts, "WaterROUTE: A model for cost optimization of industrial water supply networks when using water resources with varying salinity," *Water Res.*, vol. 202, Sep. 2021, Art. no. 117390.
[14] A. D. Gupta and K. Kulat, "Leakage reduction in water distribution system using efficient pressure management techniques. Case study: Nagpur, India," *Water Supply*, vol. 18, no. 6, pp. 2015–2027, Dec. 2018.
[15] M. Wakeel and B. Chen, "Energy consumption in urban water cycle," *Energy Proc.*, vol. 104, pp. 123–128, Dec. 2016.
[16] D. Azari, S. S. Torbaghan, H. Cappon, M. Gibescu, K. Keesman, and H. Rijnaarts, "Assessing the flexibility potential of the residential load in smart electricity grids—A data-driven approach," in *Proc. 14th Int. Conf. Eur. Energy Market (EEM)*, Jun. 2017, pp. 1–6.
[17] J. Ostergaard, C. Ziras, H. W. Bindner, J. Kazempour, M. Marinelli, P. Markussen, S. H. Rosted, and J. S. Christensen, "Energy security through demand-side flexibility: The case of Denmark," *IEEE Power Energy Mag.*, vol. 19, no. 2, pp. 46–55, Mar. 2021.
[18] M.-A. Hamidan and F. Borousan, "Optimal planning of distributed generation and battery energy storage systems simultaneously in distribution networks for loss reduction and reliability improvement," *J. Energy Storage*, vol. 46, Feb. 2022, Art. no. 103844.
[19] N. Bhusal, M. Abdelmalak, M. Kamruzzaman, and M. Benidris, "Power system resilience: Current practices, challenges, and future directions," *IEEE Access*, vol. 8, pp. 18064–18086, 2020.
[20] T. Hong, P. Pinson, Y. Wang, R. Weron, D. Yang, and H. Zareipour, "Energy forecasting: A review and outlook," *IEEE Open Access J. Power Energy*, vol. 7, pp. 376–388, Oct. 2020.
[21] S.-E. Razavi, E. Rahimi, M. S. Javadi, A. E. Nezhad, M. Lotfi, M. Shafiekhah, and J. P. S. Catalão, "Impact of distributed generation on protection and voltage regulation of distribution systems: A review," *Renew. Sustain. Energy Rev.*, vol. 105, pp. 157–167, May 2019.
[22] M. Á. Pardo, R. Cobacho, and L. Bañón, "Standalone photovoltaic direct pumping in urban water pressurized networks with energy storage in tanks or batteries," *Sustainability*, vol. 12, no. 2, p. 738, Jan. 2020.
[23] F. J. Navarro-González, M. Á. Pardo, H. E. Chabour, and T. Alskaif, "An irrigation scheduling algorithm for sustainable energy consumption in pressurised irrigation networks supplied by photovoltaic modules," *Clean Technol. Environ. Policy*, vol. 25, no. 6, pp. 2009–2024, Aug. 2023.
[24] H. M. Ramos, R. Silva Santos, P. A. López-Jiménez, and M. Pérez-Sánchez, "Multi-objective optimization tool for PATs operation in water pressurized systems," *Urban Water J.*, vol. 19, no. 6, pp. 558–568, Jul. 2022.
[25] M. A. Pardo, F. J. Navarro-González, and Y. Villacampa, "An algorithm to schedule water delivery in pressurized irrigation networks," *Comput. Electron. Agricult.*, vol. 201, Oct. 2022, Art. no. 107290.
[26] D. Fooladivanda and J. A. Taylor, "Energy-optimal pump scheduling and water flow," *IEEE Trans. Control Netw. Syst.*, vol. 5, no. 3, pp. 1016–1026, Sep. 2018.
[27] D. Fooladivanda, A. D. Domínguez-García, and P. W. Sauer, "Utilization of water supply networks for harvesting renewable energy," *IEEE Trans. Control Netw. Syst.*, vol. 6, no. 2, pp. 763–774, Jun. 2019.
[28] A. S. Zamzam, E. Dall'Anese, C. Zhao, J. A. Taylor, and N. D. Sidiropoulos, "Optimal water–power flow-problem: Formulation and distributed optimal solution," *IEEE Trans. Control Netw. Syst.*, vol. 6, no. 1, pp. 37–47, Mar. 2019.
[29] Q. Li, S. Yu, A. S. Al-Sumaiti, and K. Turitsyn, "Micro water–energy nexus: Optimal demand-side management and quasi-convex hull relaxation," *IEEE Trans. Control Netw. Syst.*, vol. 6, no. 4, pp. 1313–1322, Dec. 2019.
[30] A. Stuhlmacher and J. L. Mathieu, "Water distribution networks as flexible loads: A chance-constrained programming approach," *Electric Power Syst. Res.*, vol. 188, Nov. 2020, Art. no. 106570.
[31] A. Stuhlmacher and J. L. Mathieu, "Uncertainty-aware methods for leveraging water pumping flexibility for power networks," 2022, *arXiv:2207.04943*.
[32] A. Stuhlmacher and J. L. Mathieu, "Flexible drinking water pumping to provide multiple grid services," *Electric Power Syst. Res.*, vol. 212, Nov. 2022, Art. no. 108491.
[33] M. J. Al-Mubarak and A. J. Conejo, "Storing freshwater versus storing electricity in power systems with high freshwater electric demand," *J. Modern Power Syst. Clean Energy*, vol. 12, no. 2, pp. 323–333, 2024.
[34] A. Belmondo Bianchi, J. Willet, H. H. M. Rijnaarts, and S. Shariat Torbaghan, "Distribution robust water-based demand side management in power transmission networks," *Sustain. Energy, Grids Netw.*, vol. 36, Dec. 2023, Art. no. 101232.
[35] A. Potter, R. Haider, G. Ferro, M. Robba, and A. M. Annaswamy, "A reactive power market for the future grid," *Adv. Appl. Energy*, vol. 9, Feb. 2023, Art. no. 100114.
[36] L. Yang, Y. Xu, H. Sun, and W. Wu, "Tractable convex approximations for distributionally robust joint chance-constrained optimal power flow under uncertainty," *IEEE Trans. Power Syst.*, vol. 37, no. 3, pp. 1927–1941, May 2022.
[37] J. E. B. Iversen and P. Pinson, "RESGen: Renewable energy scenario generation platform," in *Proc. IEEE Power Eng. Soc. Gen. Meeting*, Aug. 2016, pp. 1–20.
[38] F. Pourahmadi and J. Kazempour, "Distributionally robust generation expansion planning with unimodality and risk constraints," *IEEE Trans. Power Syst.*, vol. 36, no. 5, pp. 4281–4295, Sep. 2021.
[39] A. Ratha, A. Schwele, J. Kazempour, P. Pinson, S. S. Torbaghan, and A. Virag, "Affine policies for flexibility provision by natural gas networks to power systems," *Electr. Power Syst. Res.*, vol. 189, Dec. 2020, Art. no. 106565.

[40] A. Arrigo, C. Ordoudis, J. Kazempour, Z. De Grève, J.-F. Toubeau, and F. Vallée, "Wasserstein distributionally robust chance-constrained optimization for energy and reserve dispatch: An exact and physically-bounded formulation," *Eur. J. Oper. Res.*, vol. 296, no. 1, pp. 304–322, Jan. 2022.
[41] B. K. Poolla, A. R. Hota, S. Bolognani, D. S. Callaway, and A. Cherukuri, "Wasserstein distributionally robust look-ahead economic dispatch," *IEEE Trans. Power Syst.*, vol. 36, no. 3, pp. 2010–2022, May 2021.
[42] L. Roald and G. Andersson, "Chance-constrained AC optimal power flow: Reformulations and efficient algorithms," *IEEE Trans. Power Syst.*, vol. 33, no. 3, pp. 2906–2918, May 2018.
[43] G. A. Hanasusanto, V. Roitch, D. Kuhn, and W. Wiesemann, "A distributionally robust perspective on uncertainty quantification and chance constrained programming," *Math. Program.*, vol. 151, no. 1, pp. 35–62, Jun. 2015.
[44] C. D'Ambrosio, A. Lodi, S. Wiese, and C. Bragalli, "Mathematical programming techniques in water network optimization," *Eur. J. Oper. Res.*, vol. 243, no. 3, pp. 774–788, Jun. 2015.
[45] K. Oikonomou and M. Parvania, "Optimal participation of water desalination plants in electricity demand response and regulation markets," *IEEE Syst. J.*, vol. 14, no. 3, pp. 3729–3739, Sep. 2020.
[46] L. Roald, F. Oldewurtel, B. Van Parys, and G. Andersson, "Security constrained optimal power flow with distributionally robust chance constraints," 2015, *arXiv:1508.06061*.
[47] A. J. Wood, B. F. Wollenberg, and G. B. Sheblé, *Power Generation, Operation, and Control*. Hoboken, NJ, USA: Wiley, 2013.
[48] S. P. Boyd and L. Vandenberghe, *Convex Optimization*. Cambridge, U.K.: Cambridge Univ. Press, 2004.

A. BELMONDO BIANCHI (Student Member, IEEE) received the M.S. degree in biosystems engineering with a specialization in environmental technology from Wageningen University and Research, Wageningen, The Netherlands, in 2020, where he is currently pursuing the Ph.D. degree with the Department of Environmental Technology. His research focuses on developing integrated water and electricity resource coordination mechanisms. His research interests include water technologies, power and energy systems, electricity markets, mathematical programming, and stochastic optimization.

M. A. PARDO received the M.S. degree in hydraulic engineering and the Ph.D. degree in industrial engineering from the Universidad Polit nica de Valencia, in 2008 and 2010, respectively. He has been an Associate Professor with the Department of Civil Engineering, University of Alicante, since 2011. With over a decade of teaching experience, he specializes in hydraulic engineering, energy optimization in pressure distribution networks, solar energy applications in water systems, water reuse, and sustainable water infrastructure management. He has contributed to numerous international and national research projects, collaborating with industry and earning recognition through research awards.

T. ALSKAIF (Senior Member, IEEE) received the M.Sc. degree in computer and electrical engineering from Damascus University, Damascus, Syria, in 2011, and the Ph.D. degree in computer architecture from the Statistical Analysis of Networks and Systems Research Group, Universitat Politecnica de Catalunya, Barcelona, Spain, in 2016. He is currently an Assistant Professor with the Information Technology Group, Wageningen University and Research, Wageningen, The Netherlands. His research interests include different problems in smart grids, including smart energy systems design, energy markets, and smart integration of distributed energy resources, with an emphasis on using mathematical modeling and optimization and artificial intelligence.

H. H. M. RIJNAARTS received the M.S. and Ph.D. degrees from Wageningen University and Research, Wageningen, The Netherlands, in 1987 and 1994, respectively. Since September 2009, he has held the position of a Professor of environment and water technology with the Sub-Department of Environmental Technology, Wageningen University and Research. As a renowned academic, he contributes significantly to the field of environmental technology. He is also the Director of Wageningen Institute for Environmental and Climate Research (WIMEK) and holds memberships on the boards of Deltares and the Institute for Advanced Metropolitan Solutions (AMS). His research interests include advanced biological and physical-chemical water technologies, sustainable water cycles, energy-efficient water management technologies, and environmental sustainability.

S. SHARIAT TORBAGHAN (Senior Member, IEEE) received the M.Sc. degree in electrical engineering from the Chalmers University of Technology, Gothenburg, Sweden, in 2008, and the Ph.D. degree in electrical engineering from Delft University of Technology, Delft, The Netherlands, in 2015. He is currently an Assistant Professor with the Environmental Technology Group, Wageningen University and Research, Wageningen, The Netherlands. His research interests include renewable-based energy systems modeling, infrastructure planning in a green economy, energy economics, applied statistics, optimization theory, and their applications in energy system management and analysis.